Dear Editor and referees,

Thank you for your review of our manuscript. We greatly appreciate the substantial amount of time and effort that you dedicated to this review process.

We have revised the manuscript according to your comments and the point-by-point responses are attached in this file. The marked-up manuscript version showing the changes made is also provided as follow.

Response to Referee Comment 1 on "*Rayleigh wind retrieval for the ALADIN airborne demonstrator of the Aeolus mission using simulated response calibration*"

Comments:

1. The paper shows how calibration curves for a direct-detection airborne Doppler lidar can be derived from the known pressure and temperature in the sensed atmospheric volume and a careful characterization of the transmission characteristics of the interferometers used in the receiver. The calibration procedure is a copy from what is done for AEOLUS. It is shown that the procedure can be applied as well to the airborne demonstrator of AEOLUS, and achieves a better accuracy with a reduced bias and equivalent standard deviation with collocated drop-sonde wind measurements as with a measured response curve that does not take specifically into account the pressure and temperature conditions.

   R: Thanks for your comment. It should be noted that the A2D SRRC procedure mentioned in this paper is not a pure "copy" from what is done for ALADIN. There are some significant differences, especially in the generation and update of the transmission characteristics of the FPIs of the Rayleigh receiver for the atmospheric channel. The specific differences are listed below:

   1. The transmission characteristics of FPIs for the atmospheric path are different from the transmission curves registered on the internal reference path during the instrument spectral registration because of the difference of the illumination of the beams in the atmospheric and the internal reference paths due to different divergence and incidence angles on FPIs (Reitebuch et al., 2009). As opposed to **ALADIN**, where only the transmission curve in the internal reference path can be measured during instrument spectral registration, **the A2D** FPI transmission curves both in the internal reference path and in the atmospheric path were measured in previous campaigns, demonstrating slight deviations between both transmission paths due to the aforementioned reasons. Therefore, different combinations of FPI transmission functions derived from different campaigns can be used to derive different candidate SRRCs. After the comparison of candidate SRRCs with simultaneous MRRC, the most satisfactory combination is used for initial SRRC determination.

   2. **As for ALADIN**, the core idea of the updated spectral registration using the Airy and top-hat function is based on the comparison of the predicted one and an MRRC. The FPIs transmission characteristics cannot represent the actual sensitivity of the Rayleigh receiver at the atmospheric

path until the difference of predicted and the measured responses coincide within a threshold limit. But for **A2D**, the optical path characteristic of the A2D Rayleigh channel is considered carefully. Basically, the FPI center frequency is sensitive to the incidence angle of the light. It is a reasonable way to optimize the FPI transmission function by fine adjusting the center frequency of filter A or B for the atmospheric path. The Rayleigh spectrometer is composed of two FPIs which are sequentially coupled. Thus, the reflection of the directly illuminated FPI is directed to the second FPI. Any incidence angle change in front of the Rayleigh spectrometer will act similarly on both FPIs. The related description has been added in **Sect 7 Page 21 Line 5-18.**

2. The practical significance of the method should be discussed. The paper suggests the transmission characteristics of the two FPs are very stable, except for a frequency shift caused by an incidence angle varying from one flight to the other. In Fig 10 or 13, the results are obtained with a frequency shift determined from data acquired during the same flight. Will the frequency shift be significantly modified during another flight? If yes, this should be stressed and a conclusion should be that response calibration should be done every flight.

   R: revised. Thank you for this comment. We will add a clarification to the manuscript.

   The derived frequency shift of 20 MHz can basically depend on the alignment of the atmospheric optical path. From the experience from the last 10 years it is known that this alignment is not randomly varying from flight to flight, but changes from campaign to campaign. As the telescope and optical receiver is coupled via free optical path (and not via a fibre), the mechanical integration of the A2D into the aircraft prior to each campaign leads to small variation in position and incidence angle on the spectrometers for each deployment. Thus, a valid response calibration can be used for the entire campaigns period. This is true for both, measured or rather simulated response calibrations. In order to monitor the atmospheric path alignment, the position of the spots generated on the ACCD detector behind each FPI is analyzed and serves as information on the alignment during the flight itself and among the flights during the campaigns period. It should be noted that the applied frequency shift is only 20 MHz, which is even less than the frequency separation of successive measurement points during a response calibration (25 MHz) and which corresponds to 1.8×10^{-3} of the FSR of the FPIs. The related description has been added to **Sect 5.3 Page 17 Line 14-23.**

3. The SRRC reduced the bias, but on the other hand lower the correlation coefficient with dropsonde vlos in Fig 10. This should be commented.

   R: revised. The comparison of the correlation coefficient has been added **in Sect 6 Page 18 line 5-18**: "The correlation coefficient r, bias and standard deviation are also calculated and listed in Table 5. Fig. 10 (a) illustrates the comparison of LOS wind velocity between dropsonde and A2D Rayleigh channel measurement, showing that the fit parameters slightly deviate from the ideal case. The correlation coefficient r, bias and standard deviation of the A2D Rayleigh winds are 0.95, 0.23 m s^{-1} and 2.20 m s^{-1}, respectively, which is comparable to results in previous studies (Lux et al., 2018). The comparison of LOS wind velocity between dropsonde measurements and the results derived from SRRC without FPIs optimization is illustrated in Fig. 10 (b). The corresponding correlation coefficient r, bias and standard deviation are determined to be 0.93, -3.32 m s^{-1} and 2.61 m s^{-1}, respectively. It can be seen that underestimation of the LOS wind velocity from SRRC without the FPIs optimization is significant, demonstrating the necessity of the FPIs optimization before wind retrieval when using SRRC procedure. Figure 10 (c) shows the comparison of LOS wind velocity between dropsonde measurements and results derived from SRRC with FPIs optimization. The bias is 0.05 m s^{-1}, which is better than the results from A2D wind with MRRC, and the correlation coefficient r and standard deviation are 0.94 and 2.52 m s^{-1}, respectively. This is comparable to the results from A2D Rayleigh channel measurements and implies the feasibility and robustness of SRRC with FPIs optimization on A2D Rayleigh wind retrieval. From now on, only SRRC results with optimized FPI parameters will be discussed."

4. The paper mentions the presence of an internal reference channel without explaining exactly what it is. A simple graph showing the internal reference and the atmospheric path would improve the clarity of the paper.

R: revised. Thanks for your suggestion, we didn't explain it clearly. The specific schematic of ALADIN Airborne Demonstrator (A2D) was shown in Fig. 1 in (Lux et al., 2018), which has been already referenced in the following added in **Sect 2, page 4, line 16-31** see below:

"For each direct detection wind lidar system, the emitted laser frequency should be known in order to allow an accurate derivation of the Doppler frequency shift. A zero Doppler shift reference determined by pointing to the zenith direction has been used to correct the short-term frequency drift in previous studies (Souprayen et al., 1999b; Korb et al., 1992; Dou et al., 2014). But for the A2D, the internal reference path is particularly dedicated to the derivation of information about the emitted laser frequency. As shown in Lux et al. (2018, Fig. 1), a small portion of the laser beam radiation is collected by an integrating sphere and coupled into a multi-mode fibre, then injected into the receiver via the front optics. This path is called internal reference path. The atmospheric backscattered signal is collected by a Cassegrain telescope and guided via free optical path propagation to the front optics and receiver successively. This path is called the atmospheric path. An electro-optical modulator is used to temporally separate the atmospheric signal from the internal reference signal, thereby avoiding disturbances of the internal reference signal by atmospheric signal and saturation of the detectors at short ranges (Reitebuch et al., 2009). Because of the different optical illumination of the internal and atmospheric path resulting in different divergence and incidence angles on the FPIs, the response calibration curves for these two paths are different. It is noted that the internal reference path of ALADIN is different from A2D's, where ALADIN uses free path propagation rather than fibre coupling unit."

The related descriptions of the internal reference path and atmospheric path are also updated:

1. **Sect 2.1, page 5, line 16-19**, "For ALADIN, the Rayleigh winds produced by the level 1B processor (Reitebuch et al., 2018) are based on a MRRC while the level 2B processor uses a

SRRC. A MRRC includes three response calibration curves, one each derived from the internal reference, the atmospheric and the ground return."

2. **In Sect 2.2, page 7, line 2-4**, "Regarding the A2D, a SRRC based on such a simulation approach promises an improvement in terms of wind speed errors. A SRRC includes two response calibration curves derived from internal reference path and atmospheric path."

5. Page 2, line 9: in the CDL, the backscattered light captured by the telescope is mixed with a frequency shifted emitter laser. The frequency shift enables the measurement of positive and negative winds. It is not mentioned.

   R: revised. Please see **Sect 1, page 2, line 12-13:** "…, light, and the frequency shift introduced by an acoustic-optical modulator enables the measurement of positive and negative winds."

6. Equations 3 and 4: there integrals should be between -\infty and +\infty. In practice S_a has a limited width so the limits -FSR/2 +FSR/2 can be enough if FSR is much larger, but +-\infty is better.

   R: revised. Please see the updated **Equation 3 and 4 in Sect 3, page 8, line 2-4.**

$$I_{A,B,INT}(f_i) = \int_{-\infty}^{+\infty} T_{A,B,INT}(f) S_i(f_i - f) df$$

$$I_{A,B,ATM}(f_a) = \int_{-\infty}^{+\infty} T_{A,B,ATM}(f) S_a(f_a - f) df$$

7. Page 11, lines 13-20: it is suggested the atmospheric and internal characteristics of FP transmissions are solely due to plate defects. This is wrong. The main reason is the beam étendue is different in the two channels due to a diaphragm.

   R: revised. Thanks for your comment, yes, we didn't explain it correctly at this point. It has been revised as "the transmission functions of FPIs for the atmospheric path are different from the transmission curves registered on the internal reference path during the instrument spectral registration. This is because of the difference in the illumination of the FPIs by the beams in the atmospheric and the internal reference paths, i.e. due to different divergence and incidence angles (Reitebuch et al., 2009)." Please see **Sect 2.2, page 6, line 28-31**.

8. Page 12, lines 19-23: the authors should write what \eplison_R is. It is the difference between the SRRC and the MRRC. Ideally it should be randomly fluctuations about 0 with no offset not slope.

   R: revised. The definition of ε_R has been updated in the revised manuscript as

   "ε_R is defined as the difference between response from the respective SRRCs and the MRRC. Then, the linear fit of ε_R as function of f' is made, returning a slope ε_{R_slope} and intercept $\varepsilon_{R\_intercept}$ based on Eqs. (18A) – (18B) in (Dabas and Huber, 2017). Ideally, if the results from the SRRC and MRRC match, ε_R should be randomly fluctuations about 0 with zero $\varepsilon_{R\_intercept}$ and ε_{R_slope}.", please see **Sect 5.2, page 15, line20-24.**

Response to Referee Comment 2 on "Rayleigh wind retrieval for the ALADIN airborne demonstrator of the Aeolus mission using simulated response calibration"

Major comments:

This paper presents an alternative technique for retrieving LOS wind estimates from the molecular channel of the Aeolus Airborne Demonstrator (A2D) using modeled response functions ("Simulated Rayleigh Response Calibration" or SRRC) derived using best-fit instrument models and the given atmospheric conditions (temperature and pressure) when available from other observations.

1. The SRRC approach provides some advantages over the "traditional" double-edge approach of measuring calibration response curves during the test process (the MRRC approach), but the authors could do a better job of explaining the reasoning behind this (vs. just listing numbers) at the beginning of the paper and in the abstract. The approach is a good idea, especially when faced with consistent Mie contamination during flight tests.

   R: revised.

   In the abstract, page 1, line 14-21, the reason why SRRC provides advantages over MRRC is added and revised as "…. However, differences exist between the respective atmospheric temperature profiles that are present during the conduction of the MRRC and the actual wind measurements. These differences are an important source of wind bias since the atmospheric temperature has a direct effect on the instrument response calibration. Furthermore, some experimental limitations and requirements need to be considered carefully to achieve a reliable MRRC. The atmospheric and instrumental variability thus currently limit the reliability and repeatability of a MRRC. In this paper, a procedure for a simulated Rayleigh response calibration (SRRC) is developed and presented in order to resolve these limitations of the A2D MRRC."

   In addition, related introductions are also added **in Sect.1, Page 3, line 14-24**, "Currently, only measured Rayleigh response calibrations (MRRC) are used for the A2D (Marksteiner, 2013; Lux et al., 2018; Marksteiner et al., 2018). However, the atmospheric temperature affects the Rayleigh-Brillouin line shape and has a direct effect on the instrument response calibration (Dabas et al., 2008). Differences exist between the respective atmospheric temperature profiles that are present during the conduction of the MRRC and the actual wind measurements. These differences are an important source of wind bias which grows with increasing temperature differences. This is also the reason why it is mandatory to consider the atmospheric temperature in the Aeolus level 2B procedure to retrieve reliable winds (Dabas et al., 2008; Rennie et al., 2017). Furthermore, some experimental limitations, which will be introduced specifically in Sect. 2.1, need to be considered carefully to achieve a reliable MRRC. Overall, the atmospheric and instrumental variability coming along with a MRRC limits the reliability and repeatability of A2D instrument response calibrations."

   Have other double-edge wind lidar researchers done anything similar to this before?

R: Yes, as shown in Table 1, there are several FPI-based direct detection wind lidar systems that are capable of measuring wind based on a measurement approach or a simulation approach. The black-marked parts use a simulation approach to obtain calibration response curves, which is similar to the SRRC method mentioned in this paper.

Table 1. Comparison of different FPI-based direct detection wind lidars

Lidar	Wavelength and system	Calibration approach	Instrument drift correction	References
OHP [a] Rayleigh lidar	532 nm, double FPIs	**Simulation,** FPI scanning	quick wind acquisition cycle strategy	Chanin et al., 1989; Garnier and Chanin, 1992; Souprayen et al., 1999a, 1999b
NASA [b] Rayleigh/Mie lidar	355 nm, three FPIs	**Simulation** FPI or laser scanning	locking etalon and servo-control system	Korb et al., 1992; Korb et al. 1998; Flesia and Korb, 1999; Flesia et al., 2000
USTC [c] Rayleigh lidar	355 nm, three FPIs	measurement and **simulation,** FPI scanning	locking etalon and servo-control system	Xia et al., 2012; Dou et al., 2014
ESA ALADIN	355 nm, double FPIs for Rayleigh channel	level 1B: measurement, laser scanning **level 2B: simulation,** laser scanning	internal reference path	Reitebuch et al., 2018; Rennie et al., 2017
DLR A2D	355 nm, double FPIs for Rayleigh channel	Measurement, laser scanning	internal reference path	Marksteiner, 2013; Lux et al.,2018; Marksteiner et al., 2018

[a] Observatory of Haute Provence, France

[b] National Aeronautics and Space Administration, U.S.

[c] University of Science and Technology of China, China. This lidar is mobile.

2. An explanation of the physical differences between the internal reference channel and the atmospheric channel would be helpful. For example, does the IRC have a different set of field angles into the FP etalons than provided by the telescope/receive path returns? Does the IRC only see narrowband light?

R: revised. Thanks for your suggestion, we didn't explain it clearly. Yes, the atmospheric path and internal reference path differ in their field angles. The internal reference signal is coupled into the receiver via an optical fiber whereas the atmospheric signal enters the receiver via free beam bath through a set of different optics. This leads to a slightly different set of field angles on the FPIs for the internal path and the atmospheric path. During the ISR only the internal path, illuminated with spectrally narrow-band light from the laser is recorded, while for the IRC the internal path (with narrow spectral bandwidth from the laser) and the atmospheric path with broad spectral bandwidth molecular returns, but also narrow spectral bandwidth cloud, aerosol and ground returns is recorded.

The specific schematic of ALADIN Airborne Demonstrator (A2D) was shown in Fig. 1 in (Lux et al., 2018), which has been already referenced in the following added paragraph **in Sect 2, page 4, line 16-31**, see below:

"For each direct detection wind lidar system, the emitted laser frequency should be known in order to allow an accurate derivation of the Doppler frequency shift. A zero Doppler shift reference determined by pointing to the zenith direction has been used to correct the short-term frequency drift in previous studies (Souprayen et al., 1999b; Korb et al., 1992; Dou et al., 2014). But for the A2D, the internal reference path is particularly dedicated to the derivation of information about the emitted laser frequency. As shown in Lux et al. (2018, Fig. 1), a small portion of the laser beam radiation is collected by an integrating sphere and coupled into a multi-mode fibre, then injected into the receiver via the front optics. This path is called internal reference path. The atmospheric backscattered signal is collected by a Cassegrain telescope and guided via free optical path propagation to the front optics and receiver successively. This path is called the atmospheric path. An electro-optical modulator is used to temporally separate the atmospheric signal from the internal reference signal, thereby avoiding disturbances of the internal reference signal by atmospheric signal and saturation of the detectors at short ranges (Reitebuch et al., 2009). Because of the different optical illumination of the internal and atmospheric path resulting in different divergence and incidence angles on the FPIs, the response calibration curves for these two paths are different. It is noted that the internal reference path of ALADIN is different from A2D's, where ALADIN uses free path propagation rather than fibre coupling unit."

The related descriptions of the internal reference path and atmospheric path are also updated:

1. **In Sect 2.1, page 5, line 16-19**, "For ALADIN, the Rayleigh winds produced by the level 1B processor (Reitebuch et al., 2018) are based on a MRRC while the level 2B processor uses a SRRC. A MRRC includes three response calibration curves, one each derived from the internal reference, the atmospheric and the ground return."
2. In Sect 2.2, page 6, line 25-28, "Regarding the A2D, a SRRC based on such a simulation approach promises an improvement in terms of wind speed errors. A SRRC includes two response calibration curves derived from internal reference path and atmospheric path."

3. The paper would also benefit from a short, clear discussion on the topic of Mie (aerosol)

contamination on the Rayleigh calibration as the topic comes up several times in the paper. Present the reasons for the aerosol induced bias and reference the literature. This could be followed by cleaning up some paragraphs that vaguely refer the issue, without explaining it.

R: revised. Thanks for your suggestion. About the topic of Mie contamination on Rayleigh calibration, we have updated related paragraphs.

Firstly, **in Sect 2.1, page 5, line 31 to page 6, line 1-6**, we discuss the reasons for the aerosol induced bias: “Firstly, the particulate Mie scattering which is not fully filtered out by the Fizeau interferometer will enter the FPIs and can be considered as Mie contamination of the Rayleigh signal. Because of the different spectral widths of the particle and molecular backscatter signal, the sensitivities of the FPIs on them are different. If not taken into account, the Mie contamination on the Rayleigh channel is one of the sources of systematic errors because it modifies the MRRC curve. In order to avoid such modifications, the A2D tries to conduct IRCs in preferably pure Rayleigh atmosphere.”

Then, we analyze the LOS wind velocity error induced by Mie contamination **in Sect 3 page 9 line 19-25** based on simulation results: “The LOS wind velocity error ΔV_{MC} induced by Mie contamination is defined as the difference of the LOS wind velocities measured under purely atmospheric molecular conditions and conditions with a scattering ratio of ρ. Figure 2 shows a simulation of ΔV_{MC} at T=223 K and P=301 hPa, where the x-axis and y-axis represent different response values and scattering ratios, respectively. Positive and negative ΔV_{MC} represent the overestimation and underestimation of the LOS velocity, respectively. An overestimation of LOS velocities occurs at response values less than 0.235 in this case. Larger scattering ratios result in larger overestimation, and the difference can get up to 13 m s-1 in case of $\rho = 3$.”

We also introduce the effect of Mie contamination correction on systematic error optimization in **Sect 3 page 9 line 25-27 to page 10 line 1-6**: “According to previous studies (Dabas et al., 2008), the Mie contamination correction could improve the quality of Rayleigh winds in cases of intermediate ρ, e.g. below 1.5. In this region the Mie signal is not high enough to guarantee an accurate Mie wind measurement but instead becomes rather significant for the Rayleigh channel (Sun et al., 2014; Lux et al., 2018). The value of ρ, which is needed for the Mie contamination correction in the Rayleigh channel, is obtained by analysing the Mie channel signal. The detailed algorithm can be seen in (Flamant et al., 2017). ”

Reference:

1. Flamant, P., Lever, V., Martinet, P., Flament, T., Cuesta, J., Dabas, A., Olivier, M., Huber, D.: ADM-Aeolus L2A Algorithm Theoretical Baseline Document, AE-TN-IPSL-GS-001, 5.5, 89 pp., 2017.

Specific comments:

Some additional proofreading for English language/grammar should catch some minor errors. Remaining comments listed by page/line#. A "Fair" rating is listed under Scientific Quality because it's not quite at the "Good" level with respect to referencing related work and being clear on the issues addressed, but with minor improvements as listed above and in the following comments, it will likely be above good. Overall, this is an interesting and useful paper for the field of double-edge direct detection Doppler wind lidar systems.

1. Page 2 line 24-26: This sentence describing Aeolus is awkward. Perhaps reword as "The novel combination of these two techniques, integrated for the first time into a single wind lidar, expands the observational altitude range from the ground to the lowermost 30 km of the atmosphere."
   R: revised. Please see **Sect 1 page 2, line 27-29**: "The novel combination of these two techniques, integrated for the first time into a single wind lidar, expands the observable altitude range from ground to the lowermost 30 km of the atmosphere."

   Line 29: Can delete the words, "as well" from the end of the sentence since it begins with "Furthermore".
   R: revised. Please see **Sect 1 page 3, line 1-3**: "Furthermore, as the first high spectral resolution lidar in space (Ansmann et al., 2007; Flamant et al., 2008), ALADIN has the potential to globally monitor cloud and aerosol optical properties to contribute to the climate impact studies."

2. Page 3 Line 9: Can the authors expand a little bit on the causes of "...the atmospheric and instrumental variability" for readers not familiar with the observation approach. For example, how atmospheric pressure/temperature impact the MRRC and what varies in the instrument (temperature impacting alignment? Variations in the field of view/field angles entering the etalon? Etc.?)
   R: revised. Please see **Sect 1 page 3, line 15-24, see also reply to major comment 1**

   "However, the atmospheric temperature affects the Rayleigh-Brillouin line shape and has a direct effect on the instrument response calibration (Dabas et al., 2008). Differences exist between the respective atmospheric temperature profiles that are present during the conduction of the MRRC and the actual wind measurements. These differences are an important source of wind bias which grows with increasing temperature differences. This is also the reason why it is mandatory to consider the atmospheric temperature in the Aeolus level 2B procedure to retrieve reliable winds (Dabas et al., 2008; Rennie et al., 2017). Furthermore, some experimental limitations, which will be introduced specifically in Sect. 2.1, need to be considered carefully to achieve a reliable MRRC. Overall, the atmospheric and instrumental variability coming along with a MRRC limits the reliability and repeatability of A2D instrument response calibrations."

Line 12: update to read, "It is based on an accurate theoretical model of the FPI transmission function...."

R: revised. Please see **Sect 1 page 3, line 26-27:** "It is based on an accurate theoretical model of the FPI transmission function and the molecular Rayleigh backscatter spectrum."

Line 28: edit to read, "Table one lists FPI-based direct detection wind lidar systems that are capable of measuring wind information...." Note that not all existing FPI systems that can be modeled this way are listed in the table, there are others in existence.

R: revised. Please see **Sect 2 page 4, line 12-14**: "Table 1 lists several FPI-based direct detection wind lidar systems that are capable of measuring wind information based on a measurement approach or a simulation approach."

3. Page 4 Line 10 – Should be "atmospheric conditions"

   R: revised. Please see **Sect 2.1 page 5, line 9-11:** "Regarding ground-based lidar systems, the calibration procedure can be carried out frequently. Based on stable atmospheric conditions (Dou et al., 2014; Liu et al., 2002),…"

4. Page 5 Line 19: fix to read, "...the transmission functions of the FPs for the atmospheric path are slightly different compared to ..." Then please explain why this is (physics causing the differences).

   R: revised. Please see **Sect 2.2 page 6, line 26-31.**

   "However, the transmission functions of FPIs for the atmospheric path are different from the transmission curves registered on the internal reference path during the instrument spectral registration. This is because of the difference in the illumination of the FPIs by the beams in the atmospheric and the internal reference paths, i.e. due to different divergence and incidence angles (Reitebuch et al., 2009)."

   Line 24: "regardless of measurement or simulation method, any angular alignment drift will change the incidence angles on FPIs, and hence change their transmission characteristics." Technically, the FPI transmission characteristics should be a function of incidence angles, field of view, temperature, pressure, thickness or gap length, finesse, etc. so perhaps the better term here (and elsewhere) is to say that "any angular alignment drift will change in the incidence angles on the FPIS, resulting in a different transmission value." (or something similar).

   R: revised. Thanks for your comments, it has been revised as "Furthermore, FPI transmission functions should be a function of incidence angles, field of view, temperature, pressure, thickness, fitness and so forth. Regardless of measurement or simulation method, any angular alignment drift will change the incidence angles on the FPIs, resulting in a different transmission value." Please see **Sect 2.2, page 7 line 7-10**.

5. Page 6 Line 5: This is an unusual mix of variables (wavelength and frequency shift), but ok. Line 17 and 19: The authors state that Equations 3 and 4 represent convolutions, but this is not

mathematically so. These are integrations over frequency of the product of the FPI transfer function times the specific input spectrum value at that frequency. Likewise, integrating this product over only one free spectral range implies that the authors assume there are never any signals outside the etalon FSRs (e.g. where the etalon can start to transmit again). This may be practically true for most applications/wind speeds/platform pointing motions, etc. but should at least be stated as an assumption.

R: revised. Please see the updated **Equation 3 and 4 in Sect 3, page 8, line 1-4.**

Still we state that the equation describes the convolution of the respective functions, as we first calculated the intensity values for all f_i and thus calculate a function of the transmitted intensities depending on f_i. Afterwards this function can be used to calculate the transmitted intensity for a respective frequency f_i. Thus, mathematically, this is not only the product but indeed the convolution of the respective functions.

$$I_{A,B,INT}(f_i) = \int_{-\infty}^{+\infty} T_{A,B,INT}(f) S_i(f_i - f) df$$

$$I_{A,B,ATM}(f_a) = \int_{-\infty}^{+\infty} T_{A,B,ATM}(f) S_a(f_a - f) df$$

6. Page 7 Line 5: defects could be in the FPI mirror surface(s) (plural) right?

R: revised. Please see **Sect 3, page 8 line 21-22**: "However, small defects on the FPI mirror surfaces or imperfect illumination of the FPI could result in small deviations that have to be considered (McGill et al., 1998).

Line 7: Why not also mention/reference the works of Spinhirne, McGill.

R: revised. Thanks for your suggestion, the related reference has been added in the revised manuscript. Please see **Sect 3, page 8 line 21-22**.

"However, small defects on the FPI mirror surfaces or imperfect illumination of the FPI could result in small deviations that have to be considered (McGill et al., 1998).

Reference:

McGill, M. J., and Spinhirne, J. D.: Comparison of two direct-detection Doppler lidar techniques. Opt. Eng., 37 (10), 2675-2686, https://doi.org/10.1117/1.601804, 1998.

Line 9: R is the mean reflectivity of the etalon mirrors? (again, plural?)

R: revised. Please see **Sect 3, page 9 line 3**: " R is the mean reflectivity of the mirror surfaces and,…"

Line 14: Suggest instead to say, "An easily calculated analytical expression...."

R: revised. Please see **Sect 3, page 9 line 8-10**: "An easily calculated analytical expression of the Tenti S6 line shape model for atmospherically relevant temperatures and pressures is used herein (Witschas, 2011a, b; Witschas et al., 2014)."

Lines 16-21: The paper might read more easily if this paragraph was moved up earlier in the discussion.

R: revised. The sentence "the particulate Mie scattering which is not fully filtered out by the Fizeau interferometer will enter the FPIs and can be considered as Mie contamination of the Rayleigh signal." has been moved to **Sect 2.1 Page 5 Line 31 to page 6 line 1**. We didn't change the position of the rest of the paragraph in order to read more easily, because the mentioned variables need to be described firstly.

Line 21: The "magenta" filled area appears more "pink" – perhaps use that term instead, or "light magenta"

R: revised. It has been revised as "light magenta". Please see **Sect 3 Page 9 Line 17**.

7. Page 8 Line 1: Here the authors could clarify for the readers not familiar with double edge approach why the biases are worse when Mie signal is significant but not good enough to measure winds using the Mie channel. Can this be shown somehow in Figure 2?

R: it has been revised as "According to previous studies (Dabas et al., 2008), the Mie contamination correction could improve the quality of Rayleigh winds in cases of intermediate ρ, e.g. below 1.5. In this region the Mie signal is not high enough to guarantee an accurate Mie wind measurement but instead becomes rather significant for the Rayleigh channel (Sun et al., 2014; Lux et al., 2018)." Please see **Sect 3 Page 9 Line 25-27 to Page 10 Line 1-2.**

Line 4 (paragraph 2): clarify that the procedure is done assuming no Mie interference (or otherwise?)

R: revised. Please see **Sect 3 Page 10 Line 9-10:** "It is noted that the procedure is done assuming no Mie contamination in this case."

Line 9: The text says that the red-square marks +/- 850 MHz, but the figure looks like its closer to 1 GHz. Please rectify one or the other to match.

R: Figure 3 has been updated in the revised manuscript.

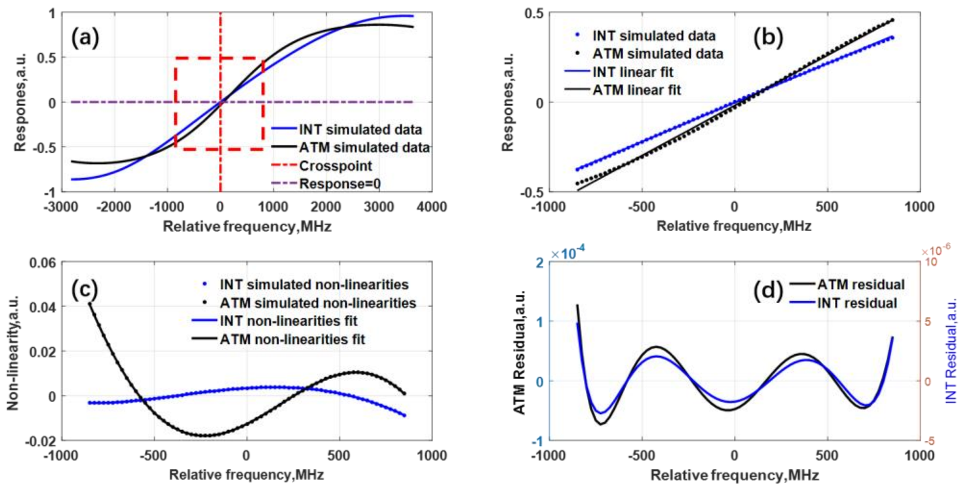

Figure 3: (a) The Simulated Rayleigh Response Calibration (SRRC) for internal reference (INT, blue line) and atmospheric return (ATM, black line), the frequency of the filter cross point is marked with a red dotted line, (b) INT (blue dots) and ATM (black dots) response and corresponding linear least squares fit (blue line for INT, black line for ATM) calibration with a frequency interval of ±850 MHz, where relative frequency is used instead of absolute frequencies, (c) the non-linearities of simulated (dots) and fitted (lines) response functions from INT (blue) and ATM (black). (d) response function residuals from INT (blue line) and ATM (black line).

Line 22: clarify that the “Then the fit of the SRRC for the internal reference and atmospheric paths can be expressed as a sum of a linear fit plus a 5th order polynomial:”

R: revised. It has been revised as “A fit of the SRRC for the internal reference and atmospheric paths can be expressed as a sum of a linear fit and a 5th order polynomial fit:” Please see **Sect 3 Page 11 Line 2-3**.

8. Page 9 Line 5: replace “In the frame of...” with “As part of..” The rest of this paragraph would benefit from additional proofreading for English grammar.

R: revised. Please see **Sect 4 Page 11 Line 12-13: “**As part of the North Atlantic Waveguide and Downstream Experiment (NAWDEX) carried out in, …”

Line 19-20: Suggest a rewrite to read “Time-space matching datasets between dropsonde and A2D can be used as both references to validated A2D wind measurements and to provide essential....”

R: revised, it has been revised as “Time-space matching datasets between dropsonde and A2D can be used as both references to validate A2D wind measurements and to provide essential atmospheric temperature and pressure profiles for SRRC in this study.” Please see **Sect 4 Page 11 Line 27-28 to page 12 line 1.**

Line 23-24: This sentence repeats a little bit of what was written before, now referring to "illumination properties" - can you be more specific? Is this a function of differences in the spatial (e.g. the pupil) distribution or in the field (e.g. angular) distribution?

R: revised. It has been revised as "The transmission functions of the FPIs are reproducible, and the transmission characteristics are different for the internal reference and atmospheric path. The underlying difference in illumination includes both a difference in the spatial as well as in the angular distribution of the light. In particular, the use of a multimode fibre in the internal reference path gives rise to speckles, resulting in an intensity distribution which is markedly different from that of atmospheric path." Please see **Sect 4 Page 12 Line 4-9.**

9. Page 10 Line 13-14: The authors state that the, "measured response values obtained from A2D wind velocity measurement mode are brought into the fitted SRRC...." What does "brought into" mean here? Is this a mapping? What is the process for doing this?

R: revised. Change "brought into…" to "combined with…", the specific process for doing this is marked with red-line square in the figure below. Please see **Sect 5 Page 13 Line 1.**

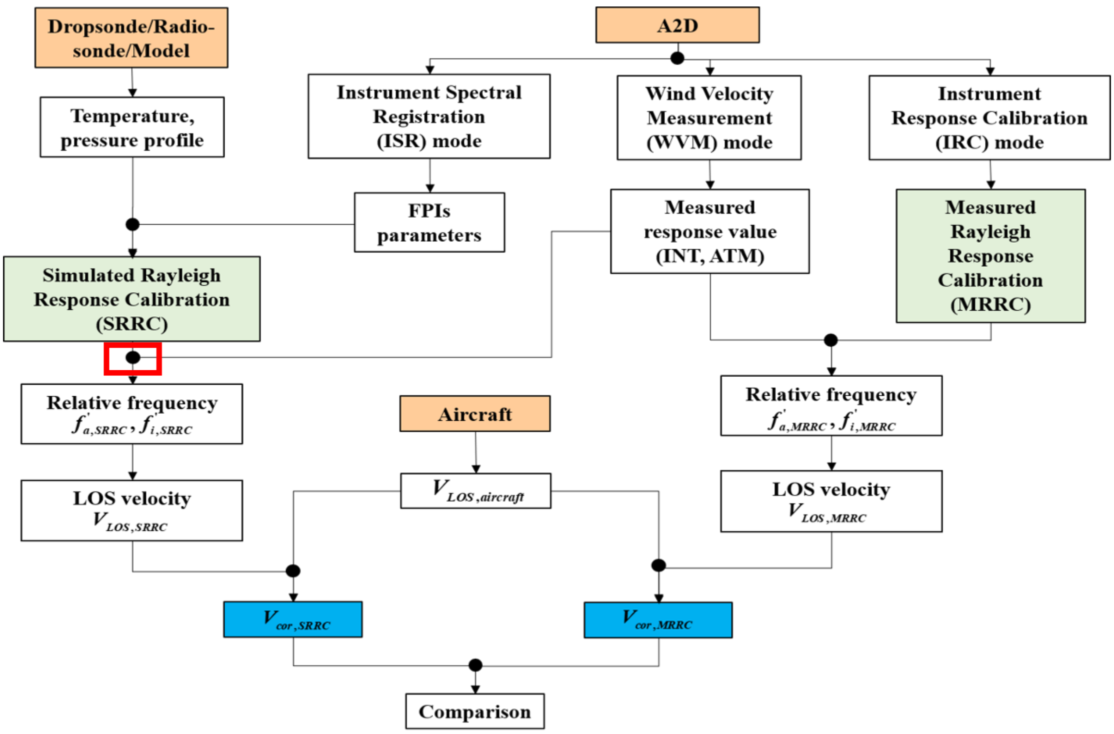

Figure 4: Flowchart of LOS velocity retrieval and comparison between A2D SRRC and MRRC.

Line 19-20: Add "and possible vertical velocity components" to the end of this first sentence.

R: revised. Please see **Sect 5 Page 13 Line 8-9:** "It is noted that LOS velocity herein includes not only the horizontal and a possible vertical wind component but also the contribution from the aircraft flight velocity."

10. Page 11 Paragraph 5.1: The figures described here would benefit from a diagram showing the campaign configuration.

R: revised. The specific parameters of FPIs during different campaigns has been listed in Table 3.

Line 8-10: This mentions of the difference between ATMG and INTG due to different illumination. The reasoning for this should be described earlier in the paper and referenced back.

R: revised. The reasoning for this has been described in **Sect 2 Page 4 Line 20-30:**

"As shown in Lux et al. (2018, Fig. 1), a small portion of the laser beam radiation is collected by an integrating sphere and coupled into a multi-mode fibre, then injected into the receiver via the front optics. This path is called internal reference path. The atmospheric backscattered signal is collected by a Cassegrain telescope and guided via free optical path propagation to the front optics and receiver successively. This path is called the atmospheric path. An electro-optical modulator is used to temporally separate the atmospheric signal from the internal reference signal, thereby avoiding disturbances of the internal reference signal by atmospheric signal and saturation of the detectors at short ranges (Reitebuch et al., 2009). Because of the different optical illumination of the internal and atmospheric path resulting in different divergence and incidence angles on the FPIs, the response calibration curves for these two paths are different."

The authors seem to change terminology back and forth throughout this section (and the corresponding figures) which makes reading the section slightly more challenging. Specifically, on page 8 the terms defined in Equations 8 and 9 are referred to as beta= sensivity and alpha=intercept, but in Figures 7 and 9 only the terms sensitivity and intercept are used. Perhaps adding the variable names beta_ATM and delta-alpha_ATM to the captions for figure7 and 9 would help. Likewise add the descriptive terms to the caption for figure 8.

R: revised.

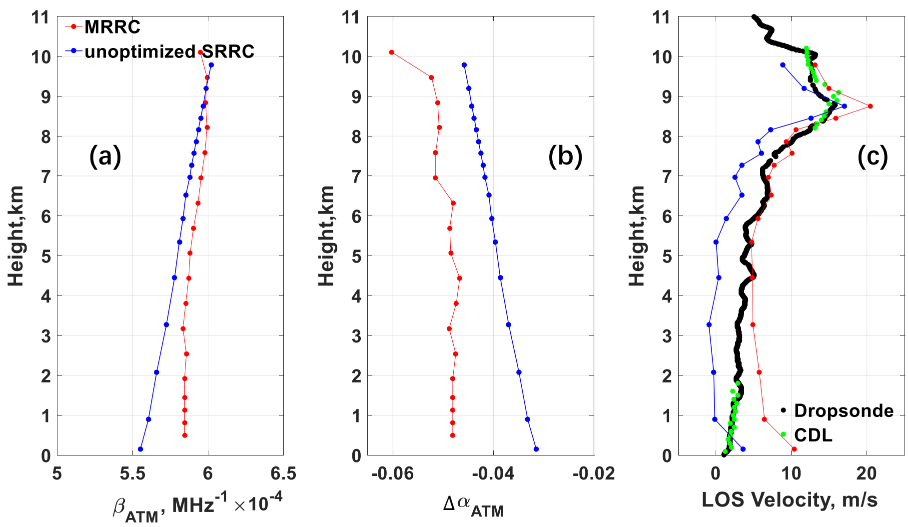

Figure 7: Case study using dropsonde data on 08:27:07 UTC, 23 September 2016: Comparison of (a) sensitivity β_{ATM} (MHz^{-1}) (b) $\Delta\alpha_{ATM}$ (c) LOS velocity between results from A2D Rayleigh channel

MRRC (red) and not optimized SRRC (blue). The LOS velocity from dropsonde (black) and CDL (green) are also presented in Fig. 7 (c).

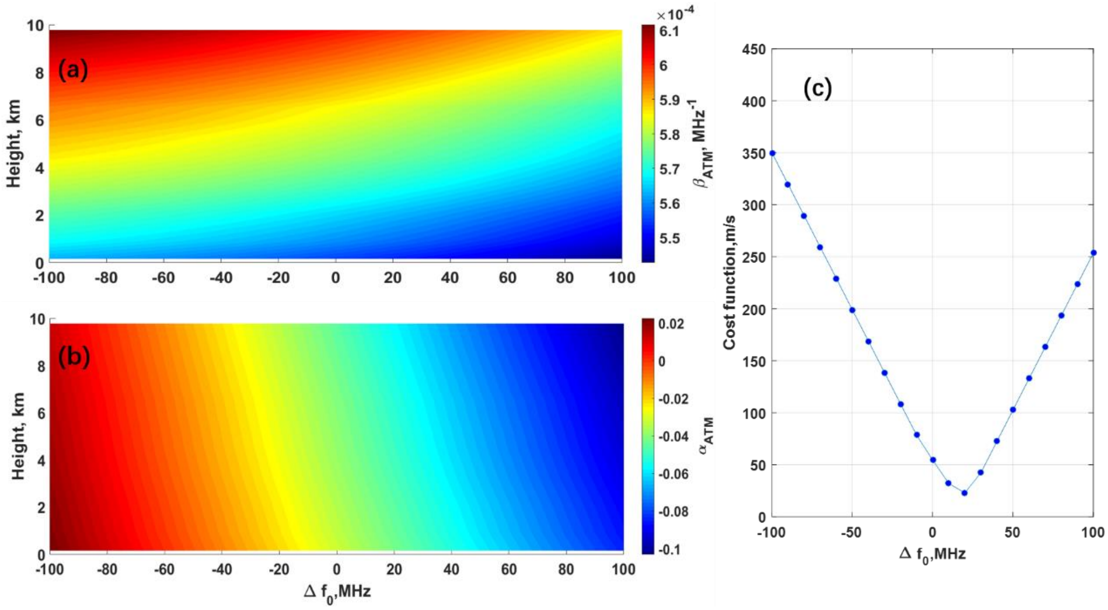

Figure 8: The effect of the centre frequency offset Δf_0 of filter A and B for atmospheric path on atmospheric response (a) $\boldsymbol{\beta}_{ATM}$ (b) $\boldsymbol{\alpha}_{ATM}$ and (c) corresponding cost function $F(\Delta f_0)$.

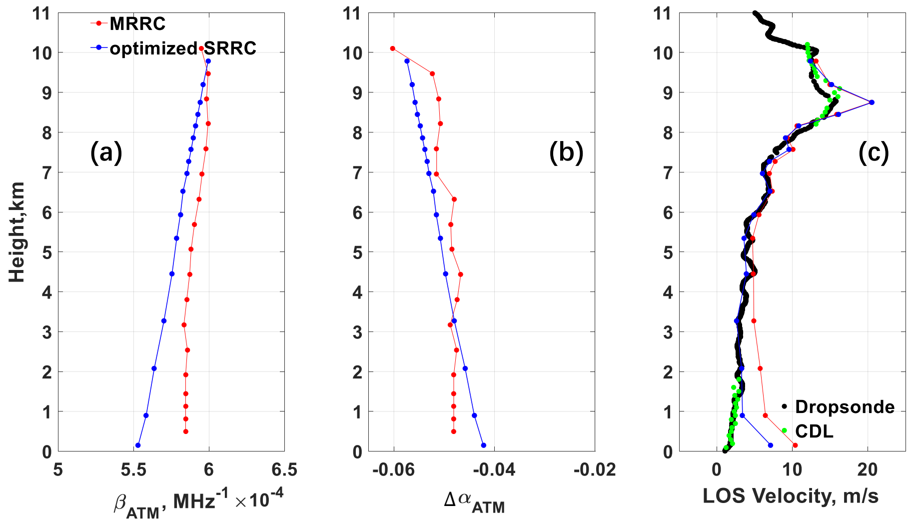

Figure 9: Case study using dropsonde data on 08:27:07 UTC, 23 September 2016: Comparison of (a) sensitivity $\boldsymbol{\beta}_{ATM}$ (MHz^{-1}) (b) $\Delta\boldsymbol{\alpha}_{ATM}$ (c) LOS velocity between results from A2D Rayleigh channel MRRC (red) and optimized SRRC (blue). The LOS velocity from dropsonde (black) and CDL (green) are also presented in Fig. 9 (c).

Line 10: What is the source of the atmospheric signal in the internal path on airborne testing (INTA)? Is there a delay in the internal reference path that causes the INTA signal to overlap with near field returns due to early overlap? Does multiple scattering play a role in these early returns?

R: revised. As the telescope and optical receiver is coupled via free optical path (and not via a fibre) the mechanical integration of the A2D inside the aircraft leads to small variation in position and incidence angle on the spectrometers for each deployment. The related description has been added in **Sect 5.1 Page 13 Line 24-27 to page 14 line 1-4**. "Specifically, the atmospheric contamination of the internal reference signal of INTA is caused by the limited suppression efficiency of the electro-optical modulator incorporated in the A2D front optics. This leads to a leakage of atmospheric backscatter being incident on the Rayleigh accumulated charge coupled device (ACCD), during the acquisition time of the internal reference signal. Please note that the internal path signal is recorded with the same ACCD detector as the atmospheric path signalusing an integration time of 4.2 μs. For the internal calibration INTG that was performed on ground, the atmospheric path was blocked manually in front of the receiver which completely avoided atmospheric contamination."

Lines 13-20: There are numerous papers discussing modeling of FPI performance. Perhaps some of these could also be referenced:

Jack A. McKay and David J. Rees "High-performance Fabry-Perot etalon mount for spaceflight," Optical Engineering 39(1), (1 January 2000). https://doi.org/10.1117/1.602361

P. D. Atherton, N K. Reay, J. Ring, and T. R. Hicks "Tunable Fabry-Perot Filters," Optical Engineering 20(6), 206806 (1 December 1981). https://doi.org/10.1117/12.7972819

J.A. McKay and David Rees , "Space-based Doppler wind lidar: Modeling of edge detection and fringe imaging Doppler analyzers"

Others by McKay, and Spinhirne, McGill, Gentry, etc.

R: revised. The related references have been added in the revised manuscript. Please see **Sect 5.2 Page 14 Line 7-8:** "The modelling of FPIs performance has been discussed in previous studies (McGill et al., 1998; McKay et al., 2000a; McKay et al., 2000b)."

References:

1. McGill, M. J., and Spinhirne, J. D.: Comparison of two direct-detection Doppler lidar techniques. Opt. Eng., 37(10), 2675-2686, https://doi.org/10.1117/1.601804, 1998.
2. McKay, J. A., and Rees, D. J.: High-performance Fabry-Perot etalon mount for spaceflight. Opt. Eng., 39 (1), 315-319, https://doi.org/10.1117/1.602361, 2000a.
3. McKay, J. A., and Rees, D.; Space-based Doppler wind lidar: modeling of edge detection and fringe imaging Doppler analyzers. Adv. Space. Res., 26(6), 883-891, https://doi.org/10.1016/S0273-1177(00)00026-0, 2000b.

Line 21: What is meant by the phrase, "Different from ALADIN"? Were the ALADIN transmission curves (internal and atmospheric paths) never measured?

R: revised. For ALADIN, only the transmission curve in the internal reference path is measured during instrument spectral registration, and the transmission curve in the atmospheric path is modelled by a convolution of an Airy function and a tilted top-hat function (Dabas and Huber, 2017).

The related description has been revised as "Different from ALADIN, where only the transmission curve in the internal reference path can be measured during instrument spectral registration, the …" Please see **Sect 5.2 Page 14 line 16-17.**

11. Page 12 Equations 15 and 17 define variables "A" and "B" for the Atmospheric and Internal paths, but this terminology is confused with the use of those variables as names for "Filter A" and "Filter B" (the two edge filters) per the labeling in Figures 1, 5, etc.

    R: revised. The variables "A", "B" in equations 15 and 17 have been revised as "M", "N", respectively. Please see **Sect 5.2 Page 14 line 27 to page 15 line 1:**

12. Page 13 Lines 11-13: This information could also be included in a previous section on the impact of angles on FPI transmission functions.

    R: revised. The related introduction has been added in revised manuscript **Sect 2.2 Page 7 line 7-10:** "Furthermore, FPI transmission functions should be a function of incidence angles, field of view, temperature, pressure, thickness, fitness and so forth. Regardless of measurement or simulation method, any angular alignment drift will change the incidence angles on the FPIs, resulting in a different transmission value."

    Line 13: "Assuming the center frequencies of filter A and B have the same offset..." Are there any challenges to this assumption? If angles get larger, does the center frequency shift more for A vs. B? A diagram (or a reference to a paper with a diagram) of the two paths through the system might help confirm that the offset is the same.

    R: revised. The related description has been added in **Sect 5.3 Page 15 Line 18-24**. "The Rayleigh spectrometer is composed of two FPIs which are sequentially coupled. Thus, the reflection of the directly illuminated first FPI is directed to the second FPI. Any incidence angle change before the Rayleigh spectrometer will act similarly on both FPIs. Considering that the initial condition was perpendicular incidence, both FPIs are affected similarly regarding a shift in the centre frequency. Furthermore, as angular shifts of only a few µrad are expected to occur, large angles do not have to be considered. Therefore, it is justified to consider the same offset for both centre frequencies induced by small incidence angle changes." The specific schematic of ALADIN Airborne Demonstrator (A2D) was shown in Fig. 1 in (Lux et al., 2018)

    Lines 15-20: The text refers to the plots in Figure 8 and talks about range gates, but the figure shows altitude bins. Which terminology should be used?

    R: revised. Replace "range gate" with "altitude bin" in the revised manuscript. Please see **Sect 5.2 Page 15 line 11-14:** "The measured responses and simulated SRRCs including fits of internal reference (red) and the 8th atmospheric altitude bin (blue dashed line, the corresponding height is around 5.7 km) are chosen as example and shown in Fig. 6."

Line 20: "all available range gates ... are used to calculate the cost function..." – does this assume there is no aerosol present in this data set?

R: revised. The related description has been added in **Sect 5.3 Page 17 Line 3-6.** "Herein all available altitude bins of SRRC from $i=1$ to $i=N$ ($N=17$) are used to calculate the cost function $F(\Delta f_0)$ for different Δf_0. It is noted that altitude bins affected by aerosol or cloud layer are hard to be flagged, unless there are auxiliary information such as CDL measurement. Therefore, these bins affected by Mie contamination are also taken into consideration in the calculation of $F(\Delta f_0)$ calculation."

13. Page 14 Lines 28-29: The sentence, "However, the temperature difference between MRRC and the actual wind measurement must..." is confusing. Perhaps the authors meant, "However, differences in the atmospheric temperature profile between when the MRRC was obtained and when the actual wind measurements were acquired are a known important source of wind bias, which are especially severe in cases of large temperature differences."

R: revised. Thanks for your suggestion, we didn't explain it accurately. It has been revised as "However, the atmospheric temperature affects the Rayleigh-Brillouin line shape and has a direct effect on the instrument response calibration (Dabas et al., 2008). Differences exist between the respective atmospheric temperature profiles that are present during the conduction of the MRRC and the actual wind measurements. These differences are an important source of wind bias which grows with increasing temperature differences.", please see **Sect 1 Page 3 line 15-19.**

Lines 21-33 (and line 11 on page 15): This issue is the basis for all the work done in this paper, right? So this should be right up front in the beginning of the paper, to help the reader understand why the work is being done and described.

R: revised. Yes, this issue is the basis of this paper. The related description has been moved to **Sect 1 Page 3 Line 14-24**, as shown below:

"Currently, only measured Rayleigh response calibrations (MRRC) are used for the A2D (Marksteiner, 2013; Lux et al., 2018; Marksteiner et al., 2018). However, the atmospheric temperature affects the Rayleigh-Brillouin line shape and has a direct effect on the instrument response calibration (Dabas et al., 2008). Differences exist between the respective atmospheric temperature profiles that are present during the conduction of the MRRC and the actual wind measurements. These differences are an important source of wind bias which grows with increasing temperature differences. This is also the reason why it is mandatory to consider the atmospheric temperature in the Aeolus level 2B procedure to retrieve reliable winds (Dabas et al., 2008; Rennie et al., 2017). Furthermore, some experimental limitations, which will be introduced specifically in Sect. 2.1, need to be considered carefully to achieve a reliable MRRC. Overall, the atmospheric and instrumental variability coming along with a MRRC limits the reliability and repeatability of A2D instrument response calibrations."

14. Page 15 Line 11: This is the key point of the paper, but it is muddled a little due to grammar. Perhaps say "This is one of the limitations of the A2D MRRC approach which can be overcome using the SRRC approach"

    R: revised. Please see **Sect 6 Page 19 line 10-11: "** ,…a and this is one of the limitations of the A2D MRRC approach which can be overcome using the SRRC approach."

    Line 15-17: Can you be more specific than saying the response calibration is affected directly? Perhaps say that the aerosol spectrum shifts the centroid of the atmospheric/filter transmission product, thereby biasing the wind speed estimates (or something like that)?

    R: revised. It has been revised and updated in **Sect 1 page 5 line 31 to page 6 line 1-6**:

    "Firstly, the particulate Mie scattering which is not fully filtered out by the Fizeau interferometer will enter the FPIs and can be considered as Mie contamination of the Rayleigh signal. Because of the different spectral widths of the particle and molecular backscatter signal, the sensitivities of the FPIs on them are different. If not taken into account, the Mie contamination on the Rayleigh channel is one of the sources of systematic errors because it modifies the MRRC curve. In order to avoid such modifications, the A2D tries to conduct IRCs in preferably pure Rayleigh atmosphere."

    Line 25: "Indeed, the Mie contamination...." – this is another key point for the paper and justification for doing the SRRC. While a detailed discussion might not be within the scope of the paper, the paper would benefit greatly from some discussion as the topic of Mie contamination comes up several time.

    R: revised. Thanks for your suggestion, we have updated related paragraphs, as shown in the reply to **Major comments #3**.

    As the basis of this paper is the effect of atmospheric temperature and pressure on calibration response curve, Mie contamination correction is not our major topic of investigation in this paper, although it is another strength of the SRRC. The other reason why we didn't discuss Mie contamination deeply in this paper is that it needs ρ value as input, and it needs to be determined with the Mie channel signal.

15. Page 16 Line 17: remove the "are" from the beginning of the line.

    R: revised. Please see **Sect 7 Page 20 line 18.**

    Line 28: "overcame" should be "overcome" here.

    R: revised. Please see **Sect 7 Page 20 line 31.**

16. Page 17 Line 1: The sentence should probably read, “Overall, the SRRC allows correction for variability in atmospheric and temperature profiles, when known, ...”

R: revised. It has been revised as “Overall, the SRRC allows correction for variability in atmospheric temperature and pressure profiles, giving accurate wind retrieval especially in cases of large atmospheric temperature differences between the acquisition time and location of the MRRC and the actual wind measurements. It can also overcome the possible ground elevation limitations, improving the accuracy of A2D wind measurements at lower altitudes. Therefore, it can improve the reliability and repeatability caused by atmospheric and instrumental variability during A2D MRRC process. Further studies based on A2D SRRC will be performed regarding the atmospheric temperature/pressure effect, Mie contamination correction and the particulate optical properties retrieval.” Please see **Sect 7 Page 21 line 19-28.**

17. Figure2: Please also use the variable name (e.g. “Rx”) with “Response” (in the caption and the axis labels)

R: revised.

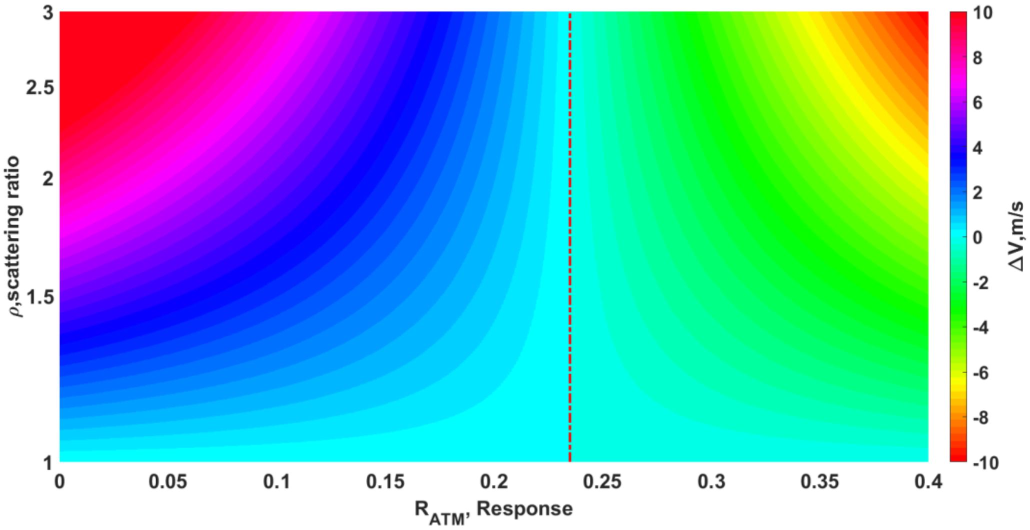

Figure 2: Simulation of LOS wind velocity errors ΔV_{MC} induced by Mie contamination and a molecular lineshape at T=223 K and P=301 hPa. The x-axis and y-axis represent the response value $\boldsymbol{R_{ATM}}$ and scattering ratio $\boldsymbol{\rho}$, respectively. The red dashed-line corresponds to the response value with minimum ΔVMC at each scattering ratio.

Figure 3: Again, refer to the variable fc when discussing the cross point frequency.

R: revised.

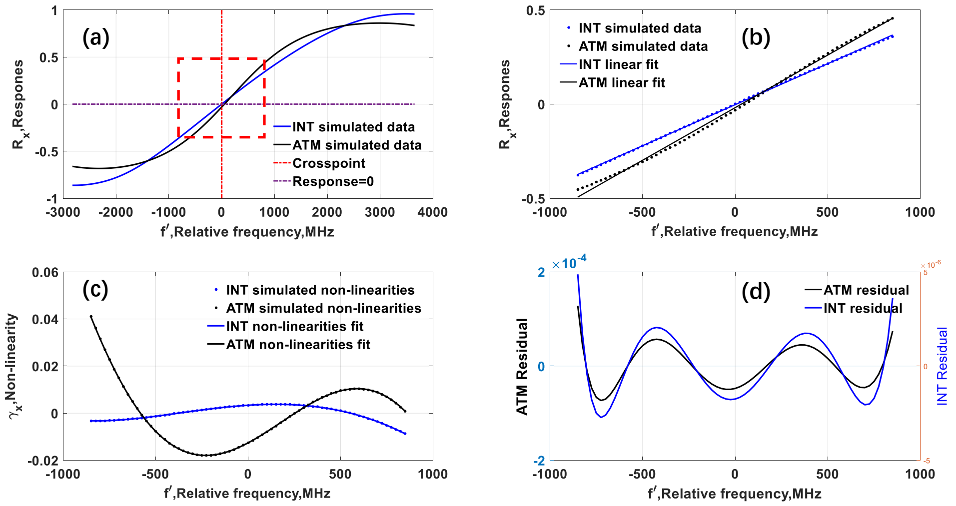

Figure 3: (a) The Simulated Rayleigh Response Calibration (SRRC) for internal reference (INT, blue line) and atmospheric return (ATM, black line), the frequency of the filter cross point is marked with a red dotted line, (b) INT (blue dots) and ATM (black dots) response and corresponding linear least squares fit (blue line for INT, black line for ATM) calibration with a frequency interval of ±850 MHz, where relative frequency is used instead of absolute frequencies, (c) the non-linearities of simulated (dots) and fitted (lines) response functions from INT (blue) and ATM (black). (d) response function residuals from INT (blue line) and ATM (black line).

Figure 5: Should the blue dashed curve be labeled “TB from INTA” (vs. TA) ?

R: revised.

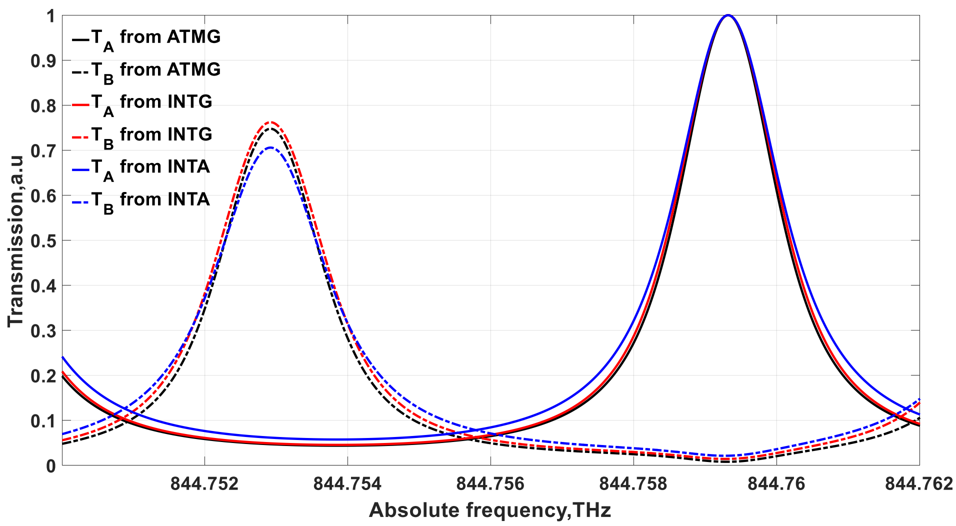

Figure 5: The fitted transmission functions of the FPIs from different campaigns, detection channels and illumination situations. The black, red and blue groups are obtained from ATM path measurement during BRAINS ground campaign (ATMG) in 2009, INT path measurement during NAWDEX from ground (INTG) in 2016 and INT path measurement during NAWDEX airborne measurement (INTA) in 2016, respectively.

Figure 6: The authors could clarify for the reader that the MRRC lines are repeated throughout the plots, e.g. say “(red and blue dashed-lines, respectively, same on every plot)”

R: revised.

Figure 9: clarify that (c) represents the retrieved LOS velocity

R: revised.

Figure 13: Can the authors say anything about the potential presence of vertical velocities and their impact on the comparison?

R: revised. Generally, the presence of vertical velocity has an effect on two main aspects:

1. During response calibration: for deriving the frequency dependency of the Rayleigh and Mie channel spectral response, a frequency scan of the laser transmitter is carried out, thus simulating well-defined Doppler shifts of the radiation backscattered from the atmosphere within the limits of the laser frequency stability. During the calibration, the contribution of (real) wind related to molecular or particular motion along the instruments’ line-of-sight (LOS) has to be eliminated, i.e. the LOS wind speed v_{LOS} needs to be zero. In practice, this is accomplished by flying curves at a roll angle of the Falcon aircraft of 20°, resulting in approximate nadir pointing of the instrument and hence $v_{LOS}\approx 0$, while assuming that the vertical wind is negligible. Consequently, regions with expectable non-zero vertical winds, e.g. introduced by gravity waves or convection, are avoided during response calibration, otherwise, it will result in incorrect response calibration curve.
2. During wind measurement: the measured LOS velocity v_{LOS} is defined as the projection of horizontal wind vector on this direction without vertical velocity contribution. When vertical velocity is not negligible, v_{LOS} is the sum of the projection of horizontal wind vector and vertical velocity.

Can the authors provide error bars on the LOS velocity retrievals? Even CDL systems have errors.

R: revised. The error bars of LOS velocity derived from MRRC and SRRC can be seen in Figure 12 (b), (c), respectively. The CDL provides high performance with accuracy of <0.3 m/s and precision of <1 m/s, respectively (Chouza, F. et al., 2016), thus we prefer to plot no error bars to the CDL measurements. Please see **Sect 6 Page 19 Line 14-15**.

An estimation of the accuracy and the precision (also considering the representativeness error estimated by means of radiosonde comparisons) can be found in Chouza et al., 2016.

Reference: Chouza, F., Reitebuch, O., Jähn, M., Rahm, S., Weinzierl, B.: Vertical wind retrieved by airborne lidar and analysis of island induced gravity waves in combination with numerical models and in situ particle measurements, Atmos. Chem. Phys., 16, 4675–4692, 2016.

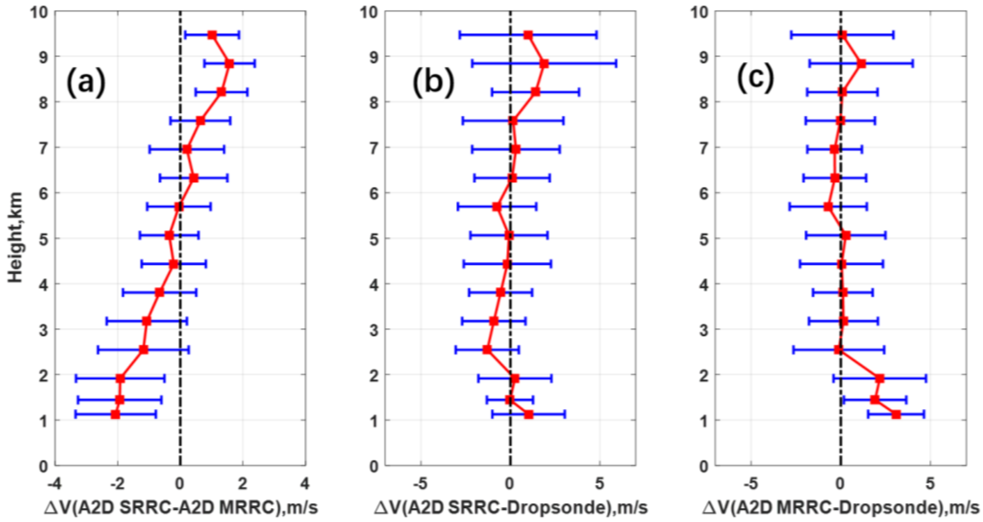

Figure 12: Comparison of profiles for LOS velocity (a) between A2D SRRC and MRRC (b) SRRC and dropsonde (c) MRRC and dropsonde.

Rayleigh wind retrieval for the ALADIN airborne demonstrator of the Aeolus mission using simulated response calibration

Xiaochun Zhai[1,2], Uwe Marksteiner[1], Fabian Weiler[1], Christian Lemmerz[1], Oliver Lux[1], Benjamin Witschas[1], Oliver Reitebuch[1]

[1]Deutsches Zentrum für Luft- und Raumfahrt e.V. (DLR), Institut für Physik der Atmosphäre, Oberpfaffenhofen 82234, Germany

[2]Ocean University of China, College of Information Science and Engineering, Ocean Remote Sensing Institute, Qingdao 266100, China

Correspondence to: Oliver. Reitebuch (Oliver.Reitebuch@dlr.de)

Abstract. Aeolus, launched on August 22nd in 2018, is the first ever satellite to directly observe wind information from the surface up to 30 km on a global scale. An airborne prototype called ALADIN Airborne Demonstrator (A2D) was developed at the German Aerospace Centre (DLR) for validating the Aeolus measurement principle based on realistic atmospheric signals. To obtain accurate wind retrievals, the A2D uses a measured Rayleigh response calibration (MRRC) to calibrate its Rayleigh channel signals. However, differences exist between ~~in~~ the respective atmospheric temperature profiles that are present during the conduction of the MRRC and the actual wind measurements~~. between when the MRRC was obtained and when the actual wind measurements were acquired~~. These differences are an important source~~s~~ of wind bias since the atmospheric temperature has a direct effect on the instrument response calibration~~atmospheric part of the MRRC~~. ~~instrument response calibratio~~ Furthermore, some experimental limitations and requirements need to be considered carefully to achieve a reliable MRRC. ~~the~~ The atmospheric and instrumental variability thus currently limit the reliability and repeatability of an~~this~~ MRRC. In this paper ~~Thus~~, a procedure for a simulated Rayleigh response calibration (SRRC) is developed and presented~~ in this paper~~ in order to resolve these limitations of the A2D ~~Rayleigh channel~~ MRRC. At first ~~T~~the transmission functions of the A2D Rayleigh channel~~ interferometer, consisting of the~~ double-edge Fabry-Perot interferometers (FPIs) in the internal reference path and atmospheric path~~,~~ are ~~firstly~~ characterised and optimized based on measurements performed during different airborne and ground-based campaigns. The optimized FPI transmission functions are~~is~~ then combined with the laser reference spectrum and the temperature dependent molecular Rayleigh backscatter spectrum to derive an accurate A2D SRRC which can finally be implemented into the~~ A2D~~ wind retrieval. Using dropsonde data as a reference, a statistical analysis based on dataset from a flight campaign in 2016 reveals a bias and a standard deviation of line-of-sight (LOS) wind speeds derived from a~~n~~ SRRC of only 0.05 $m\ s^{-1}$ and 2.52 $m\ s^{-1}$, respectively. Compared to the result derived from a~~n~~ MRRC with a bias of 0.23 $m\ s^{-1}$ and a standard deviation of 2.20 $m\ s^{-1}$, the accuracy improved while the precision is considered to be at the same level. Furthermore, it is shown that the SRRC allows the simulation of receiver responses over the whole altitude range from the aircraft down to

sea level, thus overcoming limitations due to ~~continuous~~ high~~er~~ ground elevation during the ~~performance~~ acquisition of an airborne instrument response calibrations.

1 Introduction

Continuous global wind observations are of highest priority for improving the accuracy of numerical weather prediction as well as for advancing our knowledge of atmospheric dynamics (Stoffelen et al., 2005; Weissmann et al., 2007; Žagar et al., 2008; Baker et al., 2014). Among ~~the~~ various techniques such as radiosonde, radar wind profiler, and geostationary satellite imagery, a spaceborne Doppler wind lidar is considered as the most promising one to meet the need of near-real time observations of global wind information. Based on the principle of the Doppler effect, two different wind lidar detection techniques, namely coherent and direct detection, have been developed and studied over the last decades (~~Stoffelen et al., 2005;~~ Reitebuch, 2012a). The coherent Doppler lidar (CDL), typically used in the particle-rich boundary layer, can directly determine the Doppler frequency shift via the beat signal between the emitted laser signal and the particulate backscattered light, and the frequency shift introduced by an acoustic-optical modulator enables the measurement of positive and negative winds.~~.~~ ~~Additionallythis method .~~ In contrast~~This is different,~~ for a direct detection wind lidar~~, where~~ the measured signal cannot ~~be~~ directly be related to the frequency shift. Thus, a so-called response calibration describing the relationship between the measured instrument response and the actual Doppler frequency shift constitutes a prerequisite for an accurate wind retrieval. A~~The~~ direct detection wind lidar can measure atmospheric wind by means of either particulate or molecular backscatter signals, typically offering much higher data coverage of the wind field from ground up to the lower mesosphere. Different spectral discriminators such as Fabry-Perot interferometers (Chanin et al., 1989; Korb et al., 1992), Fizeau interferometers (McKay, 1998; McKay, 2002), iodine vapor filters (Liu et al., 2002; She et al., 2007; Baumgarten, 2010; Wang et al., 2010; Hildebrand et al., 2012), Michelson interferometers (Thuillier et al., 1991; Herbst et al., 2016) and Mach-Zehnder interferometers (Bruneau, 2001; Bruneau and Pelon, 2003; Tucker et al., 2018) can be used for direct detection wind lidars.

Aeolus, launched on August 22nd, 2018, is the first ever satellite to directly observe line-of-sight (LOS) wind profiles on a global scale. ~~The~~ Its unique payload, the Atmospheric LAser Doppler INstrument (ALADIN), is a direct detection wind lidar operating at 355 nm from a 320 km orbit (Stoffelen et al., 2005; ESA, 2008; Reitebuch, 2012b). The backscatter signals from particulate and molecular backscatter are received by two different spectrometers, ~~that is,~~ which are a Fizeau interferometer in the Mie channel, measuring particulate backscatter, and ~~a spectrometer using a~~ a double-edge filter with two Fabry-Perot interferometers (FPIs) in the Rayleigh channel, measuring molecular backscatter. The novel combination of these two techniques, integrated for the first time into a single wind lidar, expands ~~which was not integrated in wind lidars before, enlarges~~ the observable~~tional~~ altitude range from ground to the lowermost 30 km of the atmosphere. ~~It~~ ALADIN provides one component of the wind vector along the instrument LOS with a vertical resolution of 0.25 km to 2 km and with a requirement on the~~and a~~ wind speed precision of 1~~2~~ m s^{-1} to 2.5 ~~4~~ ~~5~~ m s^{-1} for the horizontally projected LOS (HLOS) depending on altitude

~~(Reitebuch, 2012~~[RO1][RO2]~~)~~. Furthermore, as the first high spectral resolution lidar in space (Ansmann et al., 2007; Flamant et al., 2008), ALADIN has the potential to globally monitor cloud and aerosol optical properties to contribute to the climate impact studies~~ as well~~.

In the frame of the Aeolus program, a prototype instrument called ALADIN Airborne Demonstrator (A2D) was developed at the German Aerospace Centre (DLR). Due to its representative design and operating principle, the A2D has provided valuable information on the validation of the measurement principle from real~~istic~~ atmospheric signals before the satellite launch. In addition, the A2D is expected to contribute to the optimization of the wind measurement strategies for the satellite instrument as well as to the improvement of wind retrieval and quality control algorithms during satellite operation (Durand et al., 2006; Reitebuch et al., 2009; Paffrath et al., 2009). As the first ever airborne direct detection wind lidar, A2D has been deployed in several ground and airborne campaigns over the last 12 years (Li et al., 2010; Marksteiner, 2013; Weiler, 2017; Lux et al., 2018; Marksteiner et al., 2018).

Different instrument response calibration approaches have been studied using both measured and simulated response calibration ~~measurement and simulation~~ to characterize ~~or rather~~and calibrate the ALADIN Rayleigh channel (Tan et al., 2008; Dabas et al., 2008; Rennie et al., 2017). Currently, only measured Rayleigh response calibrations (MRRC) are used for the A2D (Marksteiner, 2013; Lux et al., 2018; Marksteiner et al., 2018). However, the atmospheric temperature affects the Rayleigh-Brillouin line shape~~,~~ and has a direct effect on the instrument response calibration (Dabas et al., 2008). Differences exist between~~ in~~ the respective atmospheric temperature profiles that are present during the conduction of~~ between when~~ the MRRC ~~was obtained~~ and ~~when~~ the actual wind measurements. These differences are~~ were acquired are~~ an important sources of wind bias~~,~~ which grows with increasing ~~are especially severe in cases of large~~ temperature differences. This is also the reason why it is mandatory to consider the atmospheric temperature in the Aeolus level 2B procedure to retrieve reliable winds (Dabas et al., 2008; Rennie et al., 2017). Furthermore, some experimental limitations, which will be introduced specifically in Sect. 2.1, need to be considered carefully to achieve a reliable MRRC. ~~at's the is considered in a dedicated correction procedure within thessor in orderRegarding the A2D specific However~~Overall, the atmospheric and instrumental variability coming along with a~~nn~~ MRRC limits the reliability and repeatability of A2D instrument response calibrations. Inspired by the calibration method used in the ALADIN level 2B processor (Dabas and Huber, 2017), the Simulated Rayleigh Response Calibration (SRRC) was developed to resolve these limitations of A2D. It is based on an accurate theoretical model of the FPI transmission function and the molecular Rayleigh backscatter spectrum. In this paper, the SRRC is introduced and its impact on the A2D wind retrieval is discussed and compared to results obtained with a measured response calibration.

In section 2, different calibration approaches of double-edge FPIs are discussed firstly~~introduced~~. Afterwards, the principle of an A2D SRRC is presented in Section 3. Section 4 gives an overview over the campaign and the dataset analysed in this paper~~Section 4 gives an overview over the airborne campaign in 2016 and the obtaineddataset analysed in this paper~~, whereas Section 5 introduces the A2D SRRC, which is applied to ~~data from a flight~~ the campaign measurements~~in 2016~~, and discusses the corresponding wind results. Section 6 provides a statistical comparison of LOS wind velocities~~y~~ from A2D Rayleigh channel measurements~~,~~ using the MRRC and -SRRC, and winds~~those~~ from simultaneous CDL and dropsonde datasets. A~~The~~ comparison of A2D MRRCs ~~instrument response calibration from A2D Rayleigh channel measurement~~ and ~~an~~ SRRCs is also evaluated in Section 6. Section 7 provides a summary and conclusion~~s~~.

2 Calibration approaches for double-edge FPIs

Chanin et al. (~~Chanin et al.,~~ 1989) demonstrated for the first time that FPIs can be used to measure wind in the middle atmosphere relying on molecular Rayleigh scattering and a laser with a ~~laser~~ wavelength of 532 nm. The so-called ~~frequency-dependent~~ response ~~calibration, which~~ can be defined as the contrast (Chanin et al., 1989) or the ratio (Korb et al., 1992) of the signal intensities obtained after transmission through the FPIs. A response calibration~~,~~ is a prerequisite for wind retrieval since it represents the relationship between the measured quantity (e.g. intensity of the backscattered light) and the frequency shift which is induced by the Doppler effect. Generally, there are two approaches to determine the relationship between response and Doppler frequency shift, ~~which is called~~ i.e. to obtain a response calibration function~~profile~~~~curve~~. Table 1 lists several FPI-based direct detection wind lidar systems ~~existing FPIs-based direct detection wind lidar systems~~ that are capable of measuring ~~to measure~~ wind information based on a measurement approach or a simulation approach. ~~Note that not all existing FPI systems that can be modelled this way are listed in Table 1.~~

For each direct detection wind lidar system, the emitted laser frequency should be known in order to allow an accurate derivation of ~~to accurately derive~~ the Doppler frequency shift. A zero Doppler shift reference determined by pointing to the zenith direction has been used to correct the short-term frequency drift in previous studies (Souprayen et al., 1999b; Korb et al., 1992; Dou et al., 2014). But for the A2D, the internal reference path is particularly dedicated to the derivation of information about the emitted laser frequency~~specially used to measure the emitted laser frequency information~~. As shown in Lux et al. (2018, Fig. 1)~~Fig. 1 in (Lux et al., 2018)~~, a small portion of the laser beam radiation is collected by an integrating sphere and coupled into a multi-mode fibre, then injected into the receiver via the front optics. This path is called internal reference path. The atmospheric backscattered signal is collected by a Cassegrain telescope and guided via free optical path propagation to the front optics and receiver successively. This path is called the atmospheric path. An electro-optical modulator is used to temporally separate the atmospheric signal from the internal reference signal, thereby avoiding disturbances of the internal reference signal by atmospheric signal and saturation of the detectors at short ranges (Reitebuch et al., 2009). ~~done having been the the internal reference signal . Thisdescribed internalal temporallythereby the~~ Because of the different ~~spectral shape~~optical illumination of the internal and atmospheric path ~~laser reference signal and atmospheric signal,~~ resulting in ~~and the~~ different divergence and incidence angles on the FPIs~~ for the internal reference path and atmospheric path~~, the response calibration curves for these two paths are different. It is noted that the internal reference path of ALADIN is different from A2D’s, where ALADIN uses free path propagation rather than fibre coupling unit.

2.1 ~~Measurement approach~~Approach using measured response calibrations

The first approach to obtain a response calibration function is based on measurements during which the laser beam is pointed into zenith direction while assuming that the vertical velocity of the probed atmospheric volume is negligible, i.e. no Doppler frequency shift is induced. Then, ~~in order to obtain the measured response calibration profile,~~ either the frequency of the laser transmitter is scanned with constant ~~over fixed~~ FPIs cavity length (Reitebuch et al., 2018; Lux et al., 2018; Marksteiner et al., 2018) or the cavity length of the FPIs is scanned while keeping the laser frequency locked (Dou et al., 2014).

Since the shape of the actual molecular Rayleigh backscatter spectrum is determined by the atmospheric temperature and pressure profiles~~conditions~~ (Tenti et al., 1974; Pan et al., 2004), the measured response calibration function~~curve~~ in the atmospheric path~~profile~~ is only valid for a specific combination of temperature and pressure profiles. Regarding ground-based lidar systems, the calibration procedure can be carried out frequently. ~~b~~Based on stable atmospheric conditions (Dou et al., 2014; Liu et al., 2002)~~, and~~ it is reasonable to assume that only small temperature and pressure ~~show only small~~ variations occur with a negligible effect on the retrieved wind within a specific analysis period. However, for spaceborne or airborne lidar systems like ALADIN or the A2D, the variability in temperature and pressure ~~would~~ can be one of the main sources of systematic errors for the Rayleigh channel wind retrieval as it modifies the instrument response calibration (Dabas et al., 2008; Marksteiner, 2013).

~~In terms of~~ For ALADIN, the Rayleigh winds produced by the level 1B processor (Reitebuch et al., 2018) are based on a~~n~~ MRRC while the level 2B processor uses a~~n~~ SRRC ~~measured atmospheric response calibration curve~~. ~~Basically,~~ A~~n~~ MRRC includes ~~two~~three response calibration curves, one each derived from the internal reference ~~path and~~ , the atmospheric and ~~eand~~ the ground return. A so-called instrument response calibration mode is usually performed once per week. During ~~these~~ about 16 minutes the frequency of the laser transmitter is scanned over 1000~~±500~~ MHz ~~(around the cross point of the FPI~~[d3]~~)~~ in steps of 25 MHz and the satellite is rolled by 35° in order to point nadir, thereby avoiding frequency shifts induced by horizontal wind velocities. ~~Furthermore, in~~In order to increase the signal to noise ratio (SNR), the signals generally from the altitude range between 6 km and 20~~16~~ km are accumulated to derive a single response calibration curve for the atmosphere (Reitebuch et al., 2018). Compared to ALADIN, the MRRC ~~atmospheric Rayleigh response calibration~~ of the A2D can be ~~obtained~~ derived and used per range-gate because of the larger SNR prevailing for airborne measurements ~~being~~ which are performed closer to their target. The instrument response calibration of the A2D can be carried out several times during a flight by tuning the laser frequency in steps of 25 MHz over a frequency interval of 1.7 GHz.

Apart from the atmospheric temperature and pressure effect on the ~~-~~MRRC~~measured response calibration profile~~, several specific experimental ~~-requirements~~constraints are critical for achieving a reliable instrument response calibration for both ALADIN and A2D. ~~some experimental limitations and requirements need to be considered carefully to achieve a reliable instrument response calibration for both ALADIN and A2D.~~ Firstly, ~~The~~ the particulate Mie scattering which is not fully filtered out by the Fizeau interferometer will enter the FPIs and can be considered as Mie contamination of the Rayleigh signal.~~,~~ Because of the different spectral widths of the particle and molecular backscatter signal, the sensitivities ~~sensitivity~~ of the FPIs on them are different~~, .~~ ~~thus~~ If not taken into account, the Mie contamination on the Rayleigh channel is one of the sources of systematic errors because it modifies the MRRC~~instrument response calibration~~ curve. ~~, which~~In order to avoid such modifications, the A2D tries to conduct IRCs in preferably ~~should be avoided to ensure the representativity of~~ pure Rayleigh ~~response~~atmosphere. Furthermore, the characteristics of the ground~~ conditions~~, such as high albedo and preferably flat terrain as well as low ground elevation, should be considered to improve the SNR, to facilitate the deduction of a ground return response curve and to maximize the vertical coverage of the atmosphere (Marksteiner, 2013; Weiler, 2017; Lux et al., 2018; Marksteiner et al., 2018). In some cases, A2D calibrations were performed over terrain with high elevation (e.g. Greenland). Obviously, no response calibration curve can be obtained from below the surface, which would however be necessary for accurate wind retrieval at other geographical locations with lower ground elevation. In addition, the LOS velocity needs to be zero during the instrument response calibration. This is accomplished by flying curves with a roll angle of 20°, which corresponds to the installation angle of the A2D telescope in the DLR Falcon 20 aircraft. Regions showing gravity wave activity or strong convection ~~should be~~are avoided as they cross the assumption of negligible vertical wind velocity (Lux et al., 2018; Marksteiner et al., 2018). Overall, the reliability and repeatability of ~~ALADIN and~~ A2D MRRCs ~~measured response calibration profile~~ is a main limitation for accurate wind retrieval.

2.2 Approach using simulated response cali~~l~~brations~~Simulation approach~~

The second approach is based on SRRC~~simulated Rayleigh response calibration profiles~~ curves and the fact that the transmitted signals through each FPI are proportional to the convolution of the respective filter transmission function with the atmospheric backscatter spectrum. Therefore, this approach relies on accurate models for both FPI transmission functions and atmospheric backscatter spectrum. In practice, the transmission function of FPIs can be obtained by scanning the laser frequency and keeping the FPI´s etalon length ~~with~~ fixed ~~FPIs~~ (Rennie et al., 2017) or scanning the spacing between the plates of FPIs with fixed laser frequency (Souprayen et al., 1999b; Xia et al., 2012).

~~In terms of~~For ALADIN and A2D, the seed laser is frequency tuneable ~~over~~ to cover a spectral range of 11 GHz in the UV to calibrate the spectral characteristics of FPIs for the internal reference path.~~,~~ ~~and this~~This procedure is called instrument spectral registration (Reitebuch et al., 2018). However, ~~since the illumination of the FPIs can be different for the internal reference and the atmospheric path (Lux et al., 2018), the transmission functions of FPIs for the atmospheric path is slightly~~ the transmission ~~characteristics~~functions of FPIs for the atmospheric path are different from the transmission curves registered on the internal reference path during the instrument spectral registration. This is because of the difference in~~of~~ the illumination of the FPIs by~~of~~ the beams in the atmospheric and the internal reference paths, i.e. due to different divergence and incidence angles ~~on FPIs~~ (Reitebuch et al., 2009).~~different compared to the one measured with the internal reference signal.~~ For ALADIN, this is taken into account by correcting the FPIs transmission curves of~~for~~ the atmospheric path (Dabas and Huber, 2017). Regarding the A2D, ~~As for A2D, Considering the limitation of A2D MRRC,~~ a~~n~~ ~~A2D~~ SRRC based on such a~~this~~ simulation approach promises an improvement in terms of ~~A2D~~ wind speed errors~~ due to the limitations of A2D MRRC~~. ~~the~~ A~~an~~ SRRC ~~also~~ includes two response calibration curves derived from internal reference path and atmospheric path~~, respectively~~. The transmission function of the A2D FPIs in the internal reference path can be obtained during an instrument spectral registration. ~~However, the~~The determination of the transmission ~~characteristics~~ functions of the FPIs in the atmospheric path of the A2D is the most sophisticated part needed to accurately retrieve ~~the~~ wind information by using ~~an~~ SRRC. –Furthermore, FPI~~s~~ transmission functions~~characteristics~~ should~~, amongst others,~~ be a function of incidence angles, field of view, temperature, pressure, thickness,~~ and,~~ fitness and so forth~~ and so forth~~. Regardless of measurement or simulation method, ~~. , any~~a~~A~~ny angular alignment drift will change ~~in~~ the incidence angles on the FPIs, resulting in a different transmission value.~~it should be noted that regardless of measurement or simulation method, any angular alignment drift will change the incidence angles on FPIs, and hence change their transmission characteristics. This will result in a change of the response calibration that has to be considered to avoid systematic errors in wind retrieval.~~ Referring to the ~~As for~~ Observatory of Haute Provence (OHP) Rayleigh lidar, the bias induced by instrument drifts can be eliminated based ~~on a quick~~ by a specific wind acquisition cycle strategy.~~,~~ ~~and the~~The ~~spectral drift can thus be removed by~~ using the differences between vertical and titled position measurement~~profiles~~ (Souprayen et al., 1999a). For ALADIN or the A2D, the instrument drift is compensated by regularly performing instrument response calibrations and instrument spectral registrations on a weekly basis~~ on a weekly basis~~.

3 The principle of A2D SRRC

The Doppler frequency shift in LOS direction is derived from the difference between the frequency of the received atmospheric return f_a and the emitted laser frequency f_i:

$$\Delta f = f_a - f_i \,, \tag{1}$$

The corresponding LOS velocity is derived from the Doppler shift equation using a laser wavelength of λ_0:

$$V_{LOS} = \frac{\lambda_0}{2} \Delta f \,, \tag{2}$$

~~For each direct detection wind lidar system, the emitted laser frequency should be known to accurately derive the Doppler frequency shift. A zero Doppler shift reference determined by pointing to the zenith direction has been used to correct the short-term frequency drift in previous studies (Souprayen et al., 1999b; Korb et al., 1992; Dou et al., 2014). But for ALADIN or A2D, the internal reference path is specially used to measure the emitted laser frequency information.~~ In order to derive f_i and f_a from the A2D Rayleigh channel, the transmitted intensit ies~~y~~ $I_{A,B,INT}(f)$ and $I_{A,B,ATM}(f)$ through the FPI~~s~~ filters A and B are used for the internal reference path (INT) and the atmospheric (ATM) path~~s are used~~, respectively:

$$\cancel{I_{A,B,INT}(f_i) = \int_{-FSR/2}^{+FSR/2} T_{A,B,INT}(f) S_i(f) df} \quad \cancel{(3)}$$

$$I_{A,B,INT}(f_i) = \int_{-\infty}^{+\infty} T_{A,B,INT}(f) S_i(f_i - f) df \,, \quad (3)$$

$$\cancel{I_{A,B,ATM}(f_a) = \int_{-FSR/2}^{+FSR/2} T_{A,B,ATM}(f) S_a(f) df} \quad \cancel{(4)}$$

$$I_{A,B,ATM}(f_a) = \int_{-\infty}^{+\infty} T_{A,B,ATM}(f) S_a(f_a - f) df \,, \quad (4)$$

$$S_a(f) = S_{RB}(f) + (\rho - 1) S_{mie}(f) \,, \quad (5)$$

~~where FSR is the free spectral range for the corresponding FPI (A or B) and measurement path (INT or ATM).~~

Taking the transmitted intensity through filter A for ~~For~~ instance, $I_{A,INT}(f_i)$ is the convolution of the filter A transmission function ~~at~~ on the internal reference path ($T_{A,INT}(f)$) and the normalized laser reference spectrum $S_i(f)$ ~~with~~ with~~of~~ the transmitted laser frequency ~~of~~ f_i. ~~,~~ ~~and~~ Accordingly, $I_{A,ATM}(f_a)$ is the convolution of the filter A transmission function on the~~at~~ atmospheric path ($T_{A,ATM}(f)$) and the normalized atmospheric backscatter signal spectrum $S_a(f)$ with ~~backscattered signal~~the centre frequency ~~of~~ f_a. $S_a(f)$ consists of the broad molecular Rayleigh backscatter spectrum $S_{RB}(f)$ (the subscript RB stands for Rayleigh–Brillouin) and the narrow particulate Mie backscatter spectrum $S_{mie}(f)$, as shown in Eq. (5). Here~~, and~~ $\rho = 1 + \beta_{aer} / \beta_{mol}$ is the scattering ratio, where β_{aer} and β_{mol} are the ~~backscattered coefficients of~~ particle and molecular backscatter coefficients, respectively.

As described by~~in~~ Garnier and Chanin (~~Garnier and Chanin,~~ 1992), the Rayleigh response~~s for internal reference or atmospheric paths are~~ is defined as:

$$R_x(f) = \frac{I_{A,x}(f) - I_{B,x}(f)}{I_{A,x}(f) + I_{B,x}(f)}, x = INT \text{ or } ATM \,, \quad (6)$$

where x represents the case of the ~~internal reference (~~ INT ~~)~~ or ~~atmospheric (~~ ATM ~~)~~ path. ~~calibration, respectively.~~

In order to determine the $R_x(f)$ by means of Eqs. (3)-(6), accurate knowledge~~s~~ about $T_{A,B,INT}(f)$, $T_{A,B,ATM}(f)$, $S_i(f)$ and $S_a(f)$ is needed. Generally, the transmission function $T(f)$ of an ideal FPI can be expressed by the Airy function. ~~, however~~ However, small defects on the FPI mirror surfaces or ~~of the~~ imperfect illumination of the FPI could result in small deviations that have to be considered ~~for an accurate analysis~~ (McGill et al., 1998). It is shown that all these defects can be represented by a Gaussian defect term ~~, modifying~~ that modifies the model of the FPI transmission function $T(f)$ to (Witschas et al., 2012):

$$T(f) = \frac{1}{FSR}\left[1 + 2\sum_{k=1}^{\infty} R^k \cos\left(\frac{2\pi k f}{FSR}\right) \exp\left(-\frac{2\pi^2 k^2 \sigma_g^2}{FSR^2}\right)\right], \qquad (7)$$

where FSR is the free spectral range of~~for~~ the corresponding FPI (A or B) ~~and~~on the respective measurement path (INT or ATM), R is the mean reflectivity of the mirror surfaces and σ_g is a defect parameter taking mirror defects into consideration.

~~$S_i(f)$ can be approximated by a Gaussian function for t~~The laser pulse line shape $S_i(f)$, with its ~~parameters~~ laser linewidth ~~parameter~~ and ~~frequency of~~ emitted laser frequency, (Lux et al., 2018; Marksteiner et al., 2018) can be approximated by a Gaussian function. The spectral distribution of $S_{mie}(f)$ is similar to $S_i(f)$ as particles can be considered to cause no significant spectral broadening due to ~~a~~ random motion. $S_{RB}(f)$ can be computed by using the Tenti S6 line shape model (Tenti et al., 1974; Pan et al., 2004) which has been widely applied in atmospheric applications. An ~~easy-processable analytical representation~~ easily calculated analytical expression of the Tenti S6 line shape model for atmospherically relevant temperatures and pressures is used herein (Witschas, 2011a, b; Witschas et al., 2014).

~~The particulate Mie scattering which is not fully filtered out by the Fizeau interferometer will enter the FPIs and can be considered as Mie contamination of the Rayleigh signal.~~ The measurement principle of the A2D Rayleigh channel signal is shown in Fig. 1 as an example for one frequency step during the instrument spectral calibration with no Doppler shift on the LOS. It is assumed that there is no Mie contamination on the Rayleigh channel in this case, that is, $\rho=1$ or $S_a(f)=S_{RB}(f)$. $S_i(f)$ is depicted using a Gaussian function with a full width at half maximum (FWHM) of 50 MHz. $S_{RB}(f)$ is calculated for T=270 K and P~~p~~=700 hPa. The transmitted integrated intensities of $S_a(f)$ through FPIs A and B, that is, $I_{A,ATM}$ and $I_{B,ATM}$ are indicated by light blue and light magenta filled areas, respectively. ~~respectively.~~

The~~The~~ LOS wind velocity error ΔV_{MC} induced by Mie contamination ΔV is defined as the difference of the LOS wind ~~velocity~~ velocities measured under purely atmospheric molecular conditions and ~~atmospheric spectral~~ conditions with a scattering ratio of ρ. Figure 2 shows a~~the~~ simulation of ΔV_{MC} at T=223 K and P=301 hPa, where the x-axis and y-axis represent different response values and scattering ratios, respectively~~, respectively~~. Positive and negative ΔV_{MC} represent the overestimation and underestimation of the LOS velocity~~, respectively~~, respectively~~in case Mie contamination is not taken into account~~. An overestimation~~e~~ of LOS velocities~~y~~ occurs at response values less than 0.235 in this case. L~~, and l~~arger scattering ratios result~~s~~ in larger overestimation, and~~.~~ t~~T~~he difference can get up to 13~~20~~ m s^{-1} in case of $\rho=3$. According to previous studies (Dabas et al., 2008), ~~it is implied that~~ the Mie contamination correction could improve the quality of Rayleigh winds in ~~the~~ cases of intermediate ρ, e.g. below 1.5~~,~~. ~~as in this case~~ In this region the Mie signal is not high enough to guarantee an accurate Mie wind measurement but ~~rather~~instead becomes rather significant for the Rayleigh channel (Sun et al., 2014; Lux et al., 2018).~~Also, it is more severe when Mie signal is significant for the Rayleigh channel but not high enough to retrieve LOS velocity from the Mie channel accurately (Sun et al., 2014; Lux et al., 2018), which is the case for low scattering values, e.g. below 1.5.~~ The value of ρ, which is needed for the Mie contamination correction in the Rayleigh channel, is obtained by analysing the Mie channel signal. The detailed algorithm can be seen in (Flamant et al., 2017). ~~As forApart fromschemeon thessthe.The~~

Following the procedure of the A2D instrument response calibration mode, the ~~transmitted~~ intensities transmitted through the FPIs and corresponding response values at each frequency ~~scan~~ step are calculated, eventually forming the SRRC of the internal reference path ($R_{INT}(f)$, blue line) and the atmospheric path ($R_{ATM}(f)$, black line) shown in Fig.~~ure~~ 3 (a). It is noted that the procedure is done assuming no Mie contamination in this case~~interference~~. The cross point frequency f_c (red dotted line) in Fig. 3 (a) is derived from $R_{INT}(f)$ where $I_{A,i}(f)-I_{B,i}(f)$ is closest to zero (Marksteiner et al., 2018). The relative frequency f' is defined as the difference between absolute frequency f and f_c. Figure 3 (b) shows the simulated response functions $R_{INT}(f')$ and $R_{ATM}(f')$ within a relative frequency interval of ± 850 MHz, where the interval corresponds~~ing~~ to the area marked by the dashed red-square ~~marked frequency area~~ in Fig. 3 (a). A linear least-squares fit $R_{linearfit\_x}(f')$ is applied to the SRRC of the internal reference and atmospheric path, ~~with~~ shown by the solid blue and black line ~~shown~~ in Fig. 3 (b). The linear fitting parameters ~~including the~~ sensitivity β_x and intercept α_x are defined as~~ below~~:

$$\beta_x = \frac{\partial R_{linearfit\_x}(f')}{\partial f'}, x = INT\ or\ ATM, \quad (8)$$

$$\alpha_x = R_{linearfit\_x}(f'=0) = R_{linearfit\_x}(f=f_c), \quad (9)$$

The non-linearity $\gamma_x(f')$ is defined as the difference between $R_x(f')$ and linear least-squares fit $R_{linearfit\_x}(f')$~~ting result~~, that is, $\gamma_x(f')=R_x(f')-(\beta_x f'+\alpha_x)$. ~~As shown in Fig. 3 (c), the~~ The different $\gamma_x(f')$ ~~characterizations~~ functions of the ~~$R_{INT}(f')$ and $R_{ATM}(f')$~~ internal reference path and the atmospheric path are shown in Fig. 3 (c) ~~clearly visible, especially for the case $R_{ATM}(f')$~~. For a wavelength of $\lambda_0 = 354.89$ nm, a LOS velocity of 1 m s^{-1} translates into a frequency shift of 5.63 MHz ~~(Lux et al, 2018)~~. Taking ~~the~~ a sensitivity $\beta_{ATM} = 5\times10^{-4}$ MHz^{-1}~~ for example~~, the atmospheric non-linearity at -200 MHz ~~can be up to nearly~~almost reaches -0.02 ~~shown in Fig. 3 (c),~~ which is equivalent to ~~magnitudes of up to~~about -40 MHz, which in turn correspond~~ing~~ to -7.1 m s^{-1}. Consequently, l~~L~~arge errors in the derived LOS velocity would occur if $\gamma_x(f')$ is not taken into account. Therefore, a 5th order polynomial fit (Marksteiner, 2013; Lux et al., 2018; Marksteiner et al., 2018) is selected to model $\gamma_x(f')$, as shown in Fig. 3 (c) for $R_{INT}(f')$ ($R_{ATM}(f')$) as solid~~in~~ blue (black) line. ~~Then the~~A fit of the SRRC for the internal reference and atmospheric paths can be expressed as a sum of a linear fit and a 5th order polynomial fit:~~,~~ ~~that is,~~ ~~Then the fitting SRRC for internal reference and atmospheric path can be expressed as:~~

$$R_{fit,x}(f') = \beta_x f' + \alpha_x + \gamma_{\cancel{fit},x}(f') = \beta_x f' + \alpha_x + \sum_{i=0}^{5} m_{i,x} f'^{i}$$

$$= (a_x + m_{0,x}) + (\beta_x + m_{1,x})f' + m_{2,x}f'^2 + m_{3,x}f'^3 + m_{4,x}f'^4 + m_{5,x}f'^5 \, , \tag{10}$$

The difference between $R_x(f')$ and $R_{fit,x}(f')$ is defined as ~~response~~ residual ~~as~~ and shown in Fig. 3 (d) for the internal reference path (blue line) and the atmospheric path (black line), respectively. A periodic fluctuation can be seen but the maximum residual of the atmospheric path is less than 1.5×10^{-4}, corresponding to 0.053 m s^{-1} for $\beta_{ATM}=5\times10^{-4}$ MHz^{-1}. The absolute difference between the two residuals (INT-ATM) is even smaller.

4 Campaign and dataset

~~In the frame of~~ As part of the North Atlantic Waveguide and Downstream Experiment (NAWDEX) carried out in 2016 in Iceland, four aircraft equipped with diverse payloads were employed to investigate the influence of diabatic processes for midlatitude weather (Schäfler et al., 2018). The DLR Falcon 20 was deployed with the A2D and a well-established 2 μm CDL, offering an ideal platform to demonstrate the ~~feasibility~~ capabilities of the A2D under complex dynamic conditions. ~~All in all~~A total of 14 research flights were performed with the Falcon aircraft during the NAWDEX campaign. The A2D was operated in ~~The~~ wind measurement mode ~~of A2D was operated~~ in most of the flight periods, while~~and~~ the instrument spectral registration mode was ~~also~~ carried out ~~during ground tests~~ on ground and during airborne measurements. Furthermore, two flights on September 28th 2016 and October 15th 2016 were carried out to obtain A2D instrument response calibrations. Six MRRCs have been performed in these two calibration flight periods. After comparison and evaluation given by Lux et al. (~~Lux et al.,~~ 2018), ~~it is concluded that~~ the 3rd calibration, which was~~is~~ carried out over an Iceland glacier on ~~12:53 UTC~~ September 28th 2016 at 12:53 UTC, is chosen as the baseline of A2D Rayleigh wind retrieval, as it shows low Rayleigh residual errors and was not affected by clouds, instrument temperature drifts and ~~other~~ outliers (Lux et al., 2018). The other three aircraft, that is, the German High Altitude and Long Range Research Aircraft (HALO), the French Service des Avions Français Instrumentés pour la Recherche en Environnement (SAFIRE) Falcon 20 and the British Facility for Airborne Atmospheric Measurements (FAAM) BAe 146, were equipped with dropsonde dispensers to provide temperature, pressure, wind and humidity profiles (Schäfler et al., 2018). Time-space matching datasets between dropsonde and A2D can be used as both references to validate A2D wind measurements and to provide ~~not only be used as reference to validate A2D wind~~

~~measurements, but also offer~~ essential atmospheric temperature and pressure profiles for SRRC in this study. Table 2 provides an overview of datasets ~~during~~ that are available from the 2016 flight campaign ~~flights~~ and are used for this study. It is noted that all matched dropsondes listed in Table 2 were dispensed from the HALO aircraft.

~~It is noted that the~~The transmission functions of the FPIs are reproducible, and the transmission characteristics are different for the internal reference and atmospheric path. ~~due to the~~The underlying difference ~~of the~~in illumination ~~of the beams in these two paths. The illumination properties difference means the difference of divergence and incidence angles on FPIs for the internal reference path and atmospheric path. It~~ [d4]~~is~~includes both a difference in the spatial as well as in the angular distribution of the light. In particular, the use of a multimode fibre in the internal reference path gives rise to speckles, resulting in an intensity distribution which is markedly different from that of atmospheric path. ~~slightly different illumination properties of the different optical paths.~~ As for the A2D instrument spectral registration during the NAWDEX campaign, the sampled transmission functions of the FPIs are~~is~~ obtained from the internal reference only ~~path rather than the atmospheric path, as~~since the atmospheric return is convolved with a temperature dependent RB spectrum and the hard target ground return would be ~~is~~ too variable due to albedo variation. The only ~~available~~ sampled transmission functions of the FPIs from the A2D atmospheric path are available from ~~for A2D was carried out in 2009 during~~ the BRillouin scattering Atmospheric INvestigation on Schneefernerhaus (BRAINS) field campaign (Witschas, 2011c; Witschas et al., 2012), which was performed during Jan-Feb 2009 to demonstrate the effect of Brillouin scattering in real atmosphere. Unique to~~at~~ BRAINS was ~~that~~ a horizontal ~~alignment~~ pointing of the outgoing laser beam ~~was used~~in order to get a hard target return of a mountain with constant albedo ~~for the atmospheric path at~~in about ~~a distance of~~ 10 km distance. ~~Therefore,~~ This allowed measurements of ~~a~~ narrowband backscatter signal through the atmospheric path ~~was measured~~. The transmission functions of the FPIs were sampled by changing the laser frequency with steps of 50 MHz over a frequency range of 12 GHz with fixed FPIs. Here, d~~D~~ifferent transmission curves of FPIs from the BRAINS field campaign in 2009 and NAWDEX airborne campaign in 2016 will be used as candidate FPIs transmission curves for SRRC analysis ~~herein~~.

5 Determination of the A2D response function and Rayleigh wind retrieval

A flowchart of the LOS wind velocity retrieval based on SRRC and MRRC is presented in Fig. 4. Firstly, the atmospheric temperature and pressure profiles are taken from dropsonde, radiosonde or model data to derive the atmospheric molecular backscattered spectrum using the analytical representation of Tenti S6 line shape model (Witschas, 2011a, b; Witschas et al., 2014). Then the transmission functions of FPIs are obtained by fitting the measured FPIs transmission characteristics based on Eq. (7). Afterwards ~~the determination of the atmospheric molecular backscatter spectrum and the transmission functions of the FPIs,~~ the frequency scan of the laser transmitter during A2D instrument response calibration is simulated to derive the SRRCs for the internal reference and the atmospheric path~~, respectively~~. The measured response values R_{ATM} , R_{INT} obtained from

A2D wind velocity measurement mode are combined with ~~are brought into~~ the ~~fitted~~ SRRC $R_{fit,ATM}(f^{'})$ and $R_{fit,INT}(f^{'})$. The Doppler frequency shift Δf_{SRRC} due to LOS velocity is then derived from the difference of $f^{'}_{a,SRRC}$ and $f^{'}_{i,SRRC}$ (Reitebuch et al., 2018):

$$\cancel{\Delta f_{SRRC} = f^{\prime}_{a,SRRC} - f^{\prime}_{i,SRRC} = \frac{R_{fit,ATM}(f^{\prime}_{a,SRRC}) - \alpha_{ATM} - \gamma_{fit,ATM}(f^{\prime}_{a,SRRC})}{\beta_{ATM}} - \frac{R_{fit,INT}(f^{\prime}_{i,SRRC}) - \alpha_{INT} - \gamma_{fit,INT}(f^{\prime}_{i,SRRC})}{\beta_{INT}}, (11)}$$

$$\Delta f_{SRRC} = f'_{a,SRRC} - f'_{i,SRRC} = \frac{R_{ATM} - \alpha_{ATM} - \gamma_{fit,ATM}(f'_{a,SRRC})}{\beta_{ATM}} - \frac{R_{INT} - \alpha_{INT} - \gamma_{fit,INT}(f'_{i,SRRC})}{\beta_{INT}}, \tag{11}$$

The LOS velocity $V_{LOS,SRRC}$ is derived ~~using the Doppler shift equation~~according to Eq. (2):

$$V_{LOS,SRRC} = \frac{\lambda_0}{2}\Delta f_{SRRC}\ , \tag{12}$$

It is noted that LOS velocity herein includes not only the horizontal and a possible vertical wind component ~~from horizontal wind~~ but also the contribution from the aircraft flight velocity~~ and possible vertical velocity component~~. The correction of the flight-induced velocity $V_{LOS,aircraft}$ is calculated using the inertial navigation system and, GPS on-board the aircraft ~~and~~ within an attitude correction algorithm (Marksteiner, 2013). Finally, the corrected LOS wind velocity $V_{cor,SRRC}$ is obtained as follows:

$$V_{cor,SRRC} = V_{LOS,SRRC} - V_{LOS,aircraft}\ , \tag{13}$$

5.1 Transmission characteristics of FPIs from different campaigns

A least-squares nonlinear procedure is applied to each sampled transmission function obtained from the BRAINS field campaign in 2009 and NAWDEX airborne campaign in 2016~~, respectively~~. Figure 5 illustrates the fits of the transmission functions where the intensities are normalized to the maximum of filter A. The black curves are~~one is~~ derived from ground-based atmospheric path (ATMG) measurements during the BRAINS field campaign in 2009. The red and blue curves represent ~~are obtained from~~ the ground-based ~~internal reference path~~ (INTG) and airborne internal reference path (INTA) measurements obtained from the ~~during~~ NAWDEX campaign in 2016, respectively. The specific parameters of FPIs are listed in Table 3. The difference between ATMG and INTG is due to the different illumination of the FPI ~~for~~ via the atmospheric and internal reference ~~optical~~ paths. ~~Also, the measurement shown by the~~ Obviously the FWHM of INTA is broader than that of INTG~~'s~~, which is most likely due to ~~a~~ small ~~slight~~ contamination by atmospheric signal ~~which is~~ not completely blocked within the A2D optical receiver. Specifically, the atmospheric contamination of the internal reference signal of INTA is caused by the limited suppression efficiency of the electro-optical modulator incorporated in the A2D front optics. This leads to a leakage of atmospheric backscatter being incident on the Rayleigh accumulated charge coupled device (ACCD), during the acquisition time of the internal reference signal. Please note that the internal path signal is recorded with the same ACCD detector as the atmospheric path signal~~, and~~using an integration time ~~temporal resolution~~ of 4.2 µs ~~is used for the internal path signal~~. For the internal calibration INTG that was performed on ground, the atmospheric path ~~the receiver~~ was blocked manually in front of the receiver ~~and only the internal reference signal is used. For that reason, there is no contamination by atmospheric signal here~~which completely avoided atmospheric contamination.

5.2 Determination of FPIs transmission functions for SRRC

The most critical part both for ALADIN and for the A2D Rayleigh response calibration is the determination of transmission curves of the FPIs for the internal reference and atmospheric paths, respectively. The modelling of FPIs performance has been ~~studied~~ discussed in ~~the~~ previous studies (McGill et al., 1998; McKay et al., 2000a; McKay et al., 2000b). As for ALADIN~~, plate defects have to be considered which lead to an asymmetric modification of the FPI transmission function in the atmospheric path. Thus~~, the FPIs transmission curve in the atmospheric path is modelled by a convolution of an Airy function, which describes the transmission of a perfect FPI, and a tilted top-hat function (~~Witschas, 2011c;~~ Dabas and Huber, 2017). The core idea of this ~~corrected spectral registration~~approach using Airy and top-hat function is based on the comparison of predicted ~~one~~ and the~~a~~ measured Rayleigh response calibration~~RRC~~. ~~MRRC.~~ The FPIs transmission characteristics cannot represent the actual sensitivity of the Rayleigh receiver at the atmospheric path until the difference of predicted and ~~the~~ measured responses coincide within a threshold limit.

Different from ALADIN, where only the transmission curve in the internal reference path can be measured during instrument spectral registration,~~,~~ the A2D FPIs transmission curves both in the internal reference path and in the atmospheric path were measured in previous campaigns. As listed in Table 4, 5 combinations of FPIs transmission functions derived from different campaigns are used to derive different SRRCs. Since there is no simultaneous dropsonde measurement to provide atmospheric temperature and pressure information for modelling the atmospheric molecular backscattered spectrum during the 3rd calibration, the radiosonde dataset at a distance of about 229 km to the calibration region (available at: http://weather.uwyo.edu/upperair/sounding.html) is used. The sensitivity β_x and intercept α_x from fitting SRRCs can give a qualitative comparison with the A2D MRRC. According to Eq. (11), the partial derivative of α_x and β_x can be obtained as follows:

$$\frac{\partial \Delta f}{\partial \alpha_{ATM}} = -\frac{1\cancel{\Delta\alpha_{ATM}}}{\beta_{ATM}}, \tag{14}$$

$$\frac{\partial \Delta f}{\partial \alpha_{INT}} = \frac{1\cancel{\Delta\alpha_{INT}}}{\beta_{INT}}, \tag{15}$$

$$\frac{\partial \Delta f}{\partial \beta_{ATM}} = \frac{\alpha_{ATM} - M\cancel{A}}{\beta_{ATM}^2}\cancel{\Delta\beta_{ATM}}, AM \equiv R_{ATM} - \gamma_{ATM}, \tag{16}$$

$$\frac{\partial \Delta f}{\partial \beta_{INT}} = \frac{N\cancel{B}-\alpha_{INT}}{\beta_{INT}^2}\cancel{\Delta\beta_{INT}}, \cancel{B}N \equiv R_{INT} - \gamma_{INT} ,$$
(17)

Using the typical values in the previous studies (Lux et al., 2018), that is, $\beta_{ATM} = 5.8\times10^{-4}$ MHz^{-1}, $\beta_{INT} = 4.5\times10^{-4}$ MHz^{-1}, $\alpha_{ATM} = -0.06$, $\alpha_{INT} = -0.001$, and assuming realistic values of $\Delta\beta_{ATM} = 10^{-5}$ MHz^{-1}, $\Delta\beta_{INT} = 10^{-5}$ MHz^{-1}, $\Delta\alpha_{ATM} = 0.01$ and $\Delta\alpha_{INT} = 0.01$, ~~which are realistic or rather probable to occur~~, it can be seen that the change of intercept $\Delta\alpha_{ATM}$ or $\Delta\alpha_{INT}$ results in frequency differences of about -17 MHz or 22 MHz, equivalent to velocity differences of -2.99 m s^{-1} or 3.91 m s^{-1}, respectively. The effect of sensitivity $\Delta\beta_{ATM}$ or $\Delta\beta_{INT}$ on velocity is related to the value of *M~~A~~* or *N~~B~~*. In the case of *~~A~~M*=0 or *~~B~~N*=0, the change of sensitivity $\Delta\beta_{ATM}$ or $\Delta\beta_{INT}$ result in frequency difference of about -1.8 MHz or 0.05 MHz, equivalent to velocity differences of -0.31 m s^{-1} or 0.009 m s^{-1}. Therefore, the retrieval of LOS wind velocity is more susceptible to intercept than sensitivity. The measured responses and simulated SRRCs including fits of internal reference (red) and the 8th ~~one~~ atmospheric ~~range gate~~altitude bin (blue dashed line, the corresponding height is around 5.7 km~~, herein the 8th bin~~) ~~is~~ are chosen as example~~, for instance~~ and ~~) from measurement and corresponding SRRCs The corresponding slopes and intercepts~~ [d5]~~are listed in Table 4 and~~ shown in Fig. 6. ~~Generally, compared to~~Comparing the intercepts of ~~the~~ measured and simulated ATM response curves~~as shown by the blue dashed line (-0.059)~~, the 1st and 3rd combination shown in Figs. 6 (a) (c) are underestimated (-0.068, -0.102, respectively), while the 2nd and 4th combination shown in Figs. 6 (b) (d) are overestimated (-0.040, -0.042, respectively). Only the 5th combination, shown in Fig. 6 (e) where the FPI parameters obtained from INTA and ATMG are used for internal reference and atmospheric response determination, shows ~~the~~ similar intercept values (-0.055).

In order to further determine which combination matches best to the actual measured Rayleigh calibration response, the procedure adopted from~~in~~ ALADIN (Dabas and Huber, 2017) is used. Herein, ε_R is defined as the difference between response from the respective SRRCs and the MRRC~~measured response calibration~~. Then, the linear fit of ε_R as function of $f^{'}$ is made, returning a slope ε_{R_slope} and intercept $\varepsilon_{R\_intercept}$ based on Eqs. (18A) – (18B) in (Dabas and Huber, 2017). Ideally, if the results from the SRRC and MRRC match~~es,~~ ε_R should be randomly fluctuations about 0 with zero $\varepsilon_{R\_intercept}$ and ε_{R_slope}. ~~there only remain Basically, if the result from the SRRC matches the measured response calibration, the slope and intercept should be as close to 0 as possible.~~ Table 4 also lists the fitting results using 5 different combinations, and it is shown that the 5th combination has second smallest absolute ε_{R_slope} ~~slope~~ and $\varepsilon_{R\_intercept}$ ~~offset~~, offering the overall consistence with the measured case. Therefore, the 5th combination will be used for initial SRRC determination.

5.3 Optimization of FPIs transmission characterization

The comparison of sensitivity and intercept of response calibration, as well as the LOS wind velocity derived from SRRC and A2D measurements, can intuitively assess the ~~the feasibility~~feasibility ~~reasonable application~~ of SRRC on A2D Rayleigh wind retrieval. Figure 7 (a) (b) shows the comparison of β_{ATM} and $\Delta\alpha_{ATM} = \alpha_{ATM} + m_{0,ATM}$ between results from SRRC and A2D Rayleigh channel measurement at 08:33:06 UTC on 23 September 2016, respectively. The LOS wind velocity results from SRRC, MRRC, simultaneous dropsonde measurements and CDL measurements are presented in Fig. 7 (c). It can be seen that β_{ATM} and $\Delta\alpha_{ATM}$ derived from SRRC have ~~the~~ similar altitude dependence as the one derived from MRRC, indicating that the atmospheric temperature and pressure effect on the response calibration is described correctly using ~~within~~ the SRRC. However, the discrepancy of $\Delta\alpha_{ATM}$ between results from SRRC and ~~measured RRC~~MRRC shown in Fig. 7 (b) is obvious, resulting in large discrepancy on LOS wind velocity between SRRC and A2D Rayleigh channel datasets shown in Fig. 7 (c). Taking data from a dropsonde which was released from HALO aircraft at the same location as reference, the LOS results from SRRC is underestimated at a height of 1 km – 8 km where it can be regarded as "clear" Rayleigh wind without Mie contamination, assuming that no aerosols are ~~prominent~~ present in this altitude. Thus, a further optimization of FPIs parameters needs to be implemented as the stability of the optical alignment of the instrument can remarkably influence~~s~~ the performance of the A2D (Reitebuch et al., 2009; Lemmerz et al., 2017; Lux et al., 2018).

Considering the optical path of the A2D Rayleigh channel, the FPI centre frequency is sensitive to the incidence angle of the light. It is a reasonable way to optimize FPI transmission function by fine adjusting the centre frequency of filter A or B for the atmospheric path. The Rayleigh spectrometer is composed of two FPIs which are sequentially coupled. Thus, the reflection of the directly illuminated first FPI is directed to the second FPI. Any incidence angle~~el~~ change before the Rayleigh spectrometer will act similarly on ~~to~~ both FPIs. Considering that the initial condition was perpendicular incidence, both FPIs are affected similarly regarding a shift in the centre frequency. Furthermore, as angular shifts of only a few µrad are expected to occur, large ~~angels~~angles do not have to be considered. ~~Considering these points,~~Therefore, it is justified to consider the same offset for both ~~the~~ centre frequencies induced by small incidence angle changes. Assuming the centre frequencies of filter A and B have the same offset Δf_0 compared to the values obtained from ATMG, that is, $\Delta f_0 = \Delta f_{0,A} = \Delta f_{0,B}$, and the FPIs parameters at the internal reference path are regarded as ideal, Figs. 8 (a) and 8 (b) present the effect of Δf_0 on the sensitivity and intercept of fitting SRRC at each ~~range gate~~altitude bin, respectively. A cost function $F(\Delta f_0)$ is defined to determine the optimized centre frequency as follows:

$$F(\Delta f_0) = \sum_{i=1}^{N} |V_{LOS,SRRC}(i) - V_{LOS,reference}(i)|, \quad (18)$$

where $V_{LOS,SRRC}(i)$ is the LOS wind velocity derived from SRRC with centre frequency offset of Δf_0 at ~~range gate~~altitude bin i, $V_{LOS,reference}(i)$ is the LOS wind velocity from simultaneous dropsonde datasets interpolated to the height of A2D Rayleigh channel ~~range gate~~altitude bin i. Herein all available ~~range gate~~altitude bins of SRRC from $i=1$ to $i=N$ ($N=17$) are used to calculate the cost function $F(\Delta f_0)$ for different Δf_0. It is noted that altitude bins affected by aerosol or cloud layer are hard to be flagged, unless there are auxiliary information such as CDL measurement. Therefore, these bins affected by Mie contamination are also taken into consideration in the calculation of $F(\Delta f_0)$ calculation.

It can be seen from Fig. 8 (c) that $F(\Delta f_0)$ has its minimum when the centre frequencies of both filter A and B for the atmospheric path increase by 20 MHz, corresponding to the optimization case for LOS wind velocity retrieval using SRRC. The profiles for β_{ATM} and $\Delta\alpha_{ATM}$ derived from SRRC with FPIs optimization are shown in Fig. 9 (a) and 9 (b), respectively. ~~Consistent with~~Compared to Figs. 8 (a) and 8 (b), the increase of centre frequency of filter A and B ($\Delta f_0 > 0$) results in decrease of β_{ATM} ~~-~~and $\Delta\alpha_{ATM}$. As shown in Fig. 9 (c), the LOS wind velocity derived from SRRC with optimized FPIs parameters now fits ~~quite well~~better to the dropsonde results except for heights below 1 km and at around 9 km where Mie contamination may negatively influence the results.

The derived frequency shift of 20 MHz can basically depend on the alignment of the atmospheric optical path. From the experience from the last 10 years it is known that this alignment is not randomly varying from flight to flight, but changes from campaign to campaign. As the telescope and optical receiver is coupled via free optical path (and not via a fibre), the mechanical integration of the A2D into the aircraft prior to each campaign leads to small variation in position and incidence angle on the spectrometers for each deployment. Thus, a valid response calibration can be used for the entire campaigns period. This is true for both, measured or rather simulated response calibrations. In order to monitor the atmospheric path alignment, the position of the spots generated on the ACCD detector behind each FPI is analysed and serves as information on the alignment during the flight itself and among the flights during the campaigns period. It should be noted that the applied frequency shift is only 20 MHz, which is even less than the frequency separation of successive measurement points during a response calibration (25 MHz) and which corresponds to 1.8×10^{-3} of the FSR of the FPIs.

~~only the respective. ·10~~

6 Statistical comparison and assessment

A~~The~~ statistical comparison~~s~~ of LOS wind velocities derived from SRRC with other instrument measurements is~~are~~ required to assess the feasibility and robustness of SRRC under various atmospheric conditions. Firstly, the quality control based on an SNR mask derived from the A2D Mie channel is applied (Marksteiner, 2013) to identify invalid winds retrieved from the

Rayleigh channel, which retains~~ing~~ a significant amount of valid Rayleigh winds ~~which were rejected by~~via a cloud and ground mask (Lux et al., 2018). Then, based on the matched dates listed in Table 2, the comparisons of LOS wind velocity from dropsonde measurements, A2D Rayleigh channel measurements, and results derived from SRRC with and without FPI optimization are illustrated in Fig. 10~~, respectively~~. A linear fit to the data points is presented to provide the slope and intercept. The correlation ~~coefficien~~coefficient *r*~~t~~, bias and standard deviation are also calculated and listed in Table 5. Fig. 10 (a) illustrates the comparison of LOS wind velocity between dropsonde and A2D Rayleigh channel measurement, showing that the fit~~ting~~ parameters slightly deviate from the ideal case. The correlation coefficient *r*, bias and standard deviation of the A2D Rayleigh winds are 0.95, 0.23 m s^{-1} and 2.20 m s^{-1}, respectively, which is comparable to results in previous studies (Lux et al., 2018). The comparison of LOS wind velocity between dropsonde measurements and the results derived from SRRC without FPIs optimization is illustrated in Fig. 10 (b). The corresponding correlation coefficient *r*, bias and standard deviation are determined to be 0.93, ~~-~~-3.32 m s^{-1} and 2.61 m s^{-1}, respectively. It can be seen that~~the~~ underestimation of the LOS wind velocity from SRRC without the FPIs optimization is significant, demonstrating the necessity of the FPIs optimization before wind retrieval when using SRRC procedure. Figure 10 (c) shows the comparison of LOS wind velocity between dropsonde measurements and results derived from SRRC with FPIs optimization. The bias is 0.05 m s^{-1}, which is better than the results from A2D wind with MRRC, and the correlation coefficient *r* and ~~-~~standard deviation are 0.94~~,~~ and ~~is~~ 2.52 m s^{-1}, respectively~~,~~. This is comparable to the results from A2D Rayleigh channel measurements ~~wind retrieval, implying~~and implies the feasibility and robustness of SRRC with FPIs optimization on A2D Rayleigh wind retrieval. From now on, only SRRC results with optimized FPI parameters will be discussed.

~~The atmospheric temperature affects the Rayleigh-Brillouin line shape, and has a direct effect on the SRRC (Dabas et al., 2008).~~ In order to evaluate the atmospheric temperature effect on response calibration procedure and wind retrieval, Figure 11 (a) shows the atmospheric temperature difference between SRRC and MRRC firstly, where the red square and blue bar represent the mean bias and standard deviation at each height. The difference of sensitivity and intercept of response calibration between SRRC and MRRC are ~~also~~ illustrated in Figs. 11 (b) (c). It can be seen from Fig. 11 (a) that larger discrepancies of atmospheric temperature can be found at about 7 km to 8 km with mean differences of less than 5 K. But for the corresponding differences of sensitivity and intercept shown in Figs. 11 (b) (c), larger discrepancies appear in lower heights, especially at heights lower than 3 km. On the one hand, it is implied~~Tthis implies~~ that the atmospheric temperature effect is less significant in the statistical analysis of 2016 flight campaign~~. However, the temperature difference between MRRC and the actual wind measurement must be considered as an important source of wind bias for the case with large temperature difference. This is the reason why it is mandatory to correct temperature for Aeolus wind retrieval in order to retrieve reliable winds (Dabas et al., 2008; Rennie et al., 2017)~~. On the other hand, due to the ground elevation ~~limitation~~ during A2D instrument response calibration, the measured response calibration below 2 km in this case cannot be obtained, thus the measured response calibration at height of 2 km are used for LOS velocity retrieval below 2 km, causing larger discrepancies shown in Figs. 11 (b) (c).

The height-dependent comparisons of LOS wind velocity from different datasets after quality control are illustrated in Fig. 12. The mean difference of LOS wind velocity between SRRC and A2D Rayleigh channel measurements shown in Fig. 12 (a) has opposite trend at lower and higher heights, which is related to the intercept difference shown in Fig. 9 (b). Similar LOS wind velocity difference tendency can be seen in Figs. 12 (b) (c) for the case between SRRC and dropsonde, and between A2D Rayleigh channel measurement and dropsonde, respectively. The error bars of LOS velocity derived from MRRC and SRRC can be also seen in Figs. 12 (b) and 12 (c), respectively. Generally, larger discrepancies occur at heights of smaller than 2 km and larger than 8 km. The LOS wind velocities derived from A2D Rayleigh channel measurements have more obvious discrepancies at heights smaller than 2 km compared to the results derived from SRRC. This is ~~,~~ consistent ~~to the results shown in Fig. 11 and 12~~ with the fact that inappropriate values of A2D calibration parameters at lower height result in additional LOS velocity bias, and this is one of the limitations of the A2D MRRC approach which can be overcome using the SRRC approach~~this is one of the limitations of A2D Rayleigh response calibration which can be overcome using SRRC~~. In order to analyse the height-dependent deviations more comprehensively, Fig. 13 shows the examples of LOS wind velocity from A2D Rayleigh channel measurement, dropsonde measurements, SRRC and CDL on 23 September 2016, where dropsonde and CDL are interpolated to the A2D height. The CDL provides high performance with accuracy of <0.3 m/s and precision of <1 m/s, respectively (Chouza, F. et al., 2016), thus we prefer to plot no error bars to the CDL measurements. Larger discrepancies can be obviously seen at heights larger than 8 km due to the occurrence of cloud layer in these cases. ~~Based on Eq. (5), when the Mie narrow spectrum with scattering ratio larger than 1 adds to the pure molecular Rayleigh-Brillouin line shape, the Rayleigh response calibration is affected directly, resulting in unrealistic LOS velocities and large systematic errors.~~

All matched CDL observations listed in Table 2 are used to assess the probability of Mie contamination on Rayleigh wind results. Figure 14 (a) shows the CDL measurement behaviour where valid (or invalid) signal is represented as 1 (or 0). The Mie contamination fraction F_{Mie} , shown in Fig. 14 (b), is defined as the ratio of the number of valid signals to all CDL observation number N (here $N=12$) at each height. Obviously, ~~the~~ F_{Mie} at heights of smaller than 2 km and between 7 km and 11 km has~~ve much~~ high~~er~~ values ~~and thus are mostly experienced by the Mie contamination compared to other heights,~~ giving the important cause for the ~~why~~ larger discrepancies~~ occur at height of less than 2 km and larger than 8 km shown~~observed in Fig. 12 and 13. It is also implied that even though quality control mentioned above is used, ~~it~~ the applied SNR threshold approach cannot guarantee the accurate removal of Rayleigh wind affected by Mie contamination.~~. Indeed, the Mie contamination correction is another strength of SRRC. However, a detailed discussion is beyond the scope of this paper.~~

7 Summary and conclusion

As the first~~ ever~~ airborne direct detection wind lidar, the A2D has been deployed in several ground and airborne campaigns over the last 12 years for validating the measurement principle of Aeolus and further improving the algorithm and measurement strategy. The A2D instrument calibration is used to obtain the response calibration ~~profile~~ function indicating the relationship between the measured signal intensities and the Doppler frequency shift which is proportional to the wind speed. However, the atmospheric and instrumental variability currently limit the reliability and repeatability of the A2D instrument response calibration. For instance, there are some factors affecting the accuracy of response calibration directly during instrument response calibration such as Mie contamination, non-zero vertical velocity, and unavailable response functions for ~~at~~ lower altitudes ~~elevation because of the elevation limitation during instrument response calibrations are usually acquired over elevated ground~~due to high ground elevation. The ~~Simulated Rayleigh Response Calibration (~~SRRC~~)~~ is thus presented in this paper to overcome these limitations of MRRC.~~measured response calibration, further demonstrating the availability and merits of SRRC.~~

The most critical part of SRRC is the determination of the transmission characteristics of FPIs for the internal reference and atmospheric paths, respectively. Different from the method used for the determination of ALADIN FPIs transmission curve in the atmospheric path where a tilted top-hat function is used, the A2D candidate SRRCs using different combinations of FPIs transmission characteristics obtained from different campaigns were calculated and compared to the ~~–~~MRRC ~~measured Rayleigh response~~ firstly. It is found that the combination of FPI parameters obtained from airborne internal reference path measurement and the ground-based atmospheric path measurement are the best to be used for the internal reference and atmospheric response determination by SRRC. Since the stability of the optical properties of the FPIs and the optical alignment of the instrument can remarkably influence the performance of the A2D, a fine tuning of FPIs centre frequency for atmospheric path is performed to optimize the SRRC parameters. It is concluded that when the centre frequencies of both filter A and B for the~~at~~ atmospheric path ~~are~~ increase by 20 MHz, the LOS wind velocity derived from SRRC provides the best consistency with the simultaneous dropsonde ~~reference~~ measurements. ~~It is noted that t~~The dropsonde profile of the wind velocity is used as reference in this study to obtain ~~is the reference quantity in this study to get~~ an optimized SRRC. ~~, and~~However, it ~~is~~would also be possible ~~potential~~ to use other references such as the ECMWF model ~~dataset and~~or 2 μm CDL measurements.

What's more, d~~D~~ropsonde data was used as a reference for statistical comparison of LOS wind velocity since it has the generally best spatiotemporal matching and coverage with the results derived from SRRC. Firstly, the biases of LOS wind velocity derived from SRRC without and with FPIs optimization are -3.32 m s^{-1} and 0.05 m s^{-1}, respectively, showing the necessity of FPIs optimization for SRRC wind retrieval. ~~Then the~~The LOS wind velocity from SRRC with FPIs optimization ~~shows that the~~also provides a standard deviation ~~is~~ of 2.52 m s^{-1}, ~~i.e.~~ showing better accuracy and comparable precision ~~compared~~ with respect to the results obtained from a conventional (measured) Rayleigh response calibration which yield~~ing~~ a bias of 0.23 m s^{-1} and standard deviation of 2.20 m s^{-1}.~~,~~ This~~thus~~ demonstrates~~ting~~ the feasibility and robustness of SRRC on A2D Rayleigh wind retrieval. Furthermore, the height-dependent statistical comparison shows that the biases caused by inappropriate calibration parameters below 2 km due to the ~~limitation~~ limiting ground elevation during ~~of elevation during~~ A2D instrument response calibrations ~~acquired over elevated ground~~ can be overcome~~overcame~~ by using SRRC, where the ~~simulation of~~ response values over the whole altitude range from the aircraft down to mean sea level can be ~~achieved~~simulated.

The larger biases at heights ~~of~~ below 2 km and above 8 km are ~~probably~~ related to residual~~the~~ Mie contamination on the Rayleigh channel. It is also shown that even though quality control based on SNR is used, ~~it cannot guarantee~~ the accurate removal of ~~the~~ points affected by Mie contamination cannot be guaranteed. This shows the necessity of combination of Mie and Rayleigh channel wind analysis.

~~Overall,~~ It should be noted that the A2D SRRC procedure mentioned in this paper is not a pure “copy” from what is done for ALADIN. There are some significant differences, especially in the generation and update of the transmission characteristics of the FPIs of the Rayleigh receiver for the atmospheric channel. Firstly, as opposed to ALADIN, where only the transmission curve in the internal reference path can be measured during instrument spectral registration, the A2D FPI transmission curves both in the internal reference path and in the atmospheric path were measured in previous campaigns, demonstrating slight deviations between both transmission paths due to the aforementioned reasons. Therefore, different combinations of FPI transmission functions derived from different campaigns can be used to derive different candidate SRRCs. After the comparison of candidate SRRCs with simultaneous MRRC, the most satisfactory combination is used for initial SRRC determination. Secondly, as for ALADIN, the core idea of the updated spectral registration using the Airy and top-hat function is based on the comparison of the predicted one and a MRRC. The FPIs transmission characteristics cannot represent the actual sensitivity of the Rayleigh receiver at the atmospheric path until the difference of predicted and the measured responses coincide within a threshold limit. But for A2D, the optical path characteristic of the A2D Rayleigh channel is considered carefully. The optimization of FPIs transmission characteristics was made by fine tuning the centre frequency of filter A or B for the atmospheric path, thus obtaining optimized SRRC.

Overall, the SRRC allows correction for variability in atmospheric temperature and pressure profiles, giving accurate wind retrieval especially in cases of large atmospheric temperature differences between the acquisition time and location of the ~~when the~~ MRRC ~~was obtained~~ and ~~when~~ the actual wind measurements ~~were acquired~~. ~~Furthermore, SRRC is more accessible as the procedure doesn’t need to meet the strict experimental requirement as MRRC’s~~. It can also overcome the possible ground elevation limitations, improving the accuracy of A2D wind measurements at lower altitudes. Therefore, ~~the SRRC allows correcting for the atmospheric temperature and pressure profiles, and the possible ground elevation limitations and can, hence, improve the accuracy of A2D wind measurements especially at lower altitudes. It~~ it can improve the reliability and repeatability ~~limitations~~ caused by atmospheric and instrumental variability ~~and constraints~~ during A2D ~~instrument response calibration measurement~~MRRC process. Further studies based on A2D SRRC will be performed regarding the atmospheric temperature/pressure effect, Mie contamination correction and the particulate optical properties retrieval.

Data availability. Data used in this paper can be provided upon request by email to Oliver Reitebuch (oliver.reitebuch@dlr.de).

Competing interests. The authors declare that they have no conflict of interest

Acknowledgements. The development of the ALADIN Airborne Demonstrator and the airborne campaigns were supported by the German Aerospace Center (Deutsches Zentrum für Luft- und Raumfahrt e.V., DLR) and the European Space Agency (ESA), providing funds related to the preparation of Aeolus (WindVal II, contract no. 4000114053/15/NL/FF/gp). The first author was funded by the Chinese Scholarship Council (CSC number: 201706330031).

References

Ansmann, A., Wandinger, U., Le Rille, O., Lajas, D., and Straume, A. G.: Particulate backscatter and extinction profiling with the spaceborne high-spectral-resolution Doppler lidar ALADIN: methodology and simulations, Appl. Opt., 46, 6606-6622, https://doi.org/10.1364/AO.46.006606, 2007.

Baker, W. E., Atlas, R., Cardinali, C., Clement, A., Emmitt, G. D., Gentry, B. M., Hardesty, R. M., Källén, E., Kavaya, M. J., Langland, R., Ma, Z., Masutani, M., Mccarty, W., Pierce, R. B., Pu, Z., Riishojgaard, L. P., Ryan, J., Tucker, S., Weissmann, M., Yoe, J. G.~~... & Ma, Z., ... & Ma, Z.~~: Lidar-measured wind profiles: The missing link in the global observing system, Bulletin of the American Meteorological Society, 95(4), 543-564, , 2014.

Baumgarten, G.: Doppler Rayleigh/Mie/Raman lidar for wind and temperature measurements in the middle atmosphere up to 80 km, Atmos. Meas. Tech., 3, 1509-1518, https://doi.org/10.5194/amt-3-1509-2010, 2010.

Bruneau, D.: Mach–Zehnder interferometer as a spectral analyzer for molecular Doppler wind lidar, Appl. Opt., 40, 391-399, https://doi.org/10.1364/AO.40.000391, 2001.

Bruneau, D., and Pelon, J.: Simultaneous measurements of particle backscattering and extinction coefficients and wind velocity by lidar with a Mach–Zehnder interferometer: principle of operation and performance assessment, Appl. Opt., 42, https://doi.org/10.1364/AO.42.001101, 1101-1114, 2003.

Chanin, M. L., Garnier, A., Hauchecorne, A., and Porteneuve, J.: A Doppler lidar for measuring winds in the middle atmosphere, Geophys. Res. Lett., 16, 1273-1276, https://doi.org/10.1029/GL016i011p01273, 1989.

Chouza, F., Reitebuch, O., Jähn, M., Rahm, S., Weinzierl, B.: Vertical wind retrieved by airborne lidar and analysis of island induced gravity waves in combination with numerical models and in situ particle measurements, Atmos. Chem. Phys., 16, 4675–4692, 2016.

Dabas, A., Denneulin, M. L., Flamant, P., Loth, C., Garnier, A., and Dolfi-Bouteyre, A.: Correcting winds measured with a Rayleigh Doppler lidar from pressure and temperature effects, Tellus A: Dyn. Meteorol. Oceanogr., 60, 206-215, https://doi.org/10.1111/j.1600-0870.2007.00284.x, 2008.

Dabas, A., and Huber, D.: Generation and update of AUX_CSR, AE-TN-MFG-L2P-CAL-003, 4.0, 43 pp, 2017.

Dou, X., Han, Y., Sun, D., Xia, H., Shu, Z., Zhao, R., Shangguan, M., and Guo, J.: Mobile Rayleigh Doppler lidar for wind and temperature measurements in the stratosphere and lower mesosphere, Opt. Express, 22, A1203-A1221, https://doi.org/10.1364/OE.22.0A1203, 2014.

Durand, Y., Chinal, E., Endemann, M., Meynart, R., Reitebuch, O., and Treichel, R.: ALADIN airborne demonstrator: a Doppler Wind lidar to prepare ESA's ADM-Aeolus Explorer mission, in: Proceedings of Earth Observing Systems XI. International Society for Optics and Photonics, San Diego, California, United States, September 2006.

ESA.: ADM-Aeolus: Science Report, ESA Communication Production Office, 2008.

Flamant, P., Cuesta, J., Denneulin, M. L., Dabas, A., and Huber, D.: ADM-Aeolus retrieval algorithms for aerosol and cloud products, Tellus A: Dyn. Meteorol. Oceanogr., 60, 273-286, https://doi.org/10.1111/j.1600-0870.2007.00287.x, 2008.

Flamant, P., Lever, V., Martinet, P., Flament, T., Cuesta, J., Dabas, A., Olivier, M., Huber, D.: ADM-Aeolus L2A Algorithm Theoretical Baseline Document, AE-TN-IPSL-GS-001, 5.5, 89 pp., 2017.

Flesia, C., and Korb, C. L.: Theory of the double-edge molecular technique for Doppler lidar wind measurement, Appl. Opt., 38, https://doi.org/10.1364/AO.38.000432, 432-440, 1999.

Flesia, C., Korb, C. L., & Hirt, C.: Double-edge molecular measurement of lidar wind profiles at 355 nm, Opt. Lett., 25, 1466-1468, https://doi.org/10.1364/OL.25.001466, 2000.

Garnier, A., and Chanin, M. L.: Description of a Doppler Rayleigh lidar for measuring winds in the middle atmosphere, Appl. Phys. B, 55, 35-40, https://doi.org/10.1007/BF00348610, 1992.

Gentry, B. M., H. Chen, S. X. Li (2000): Wind measurements with 355-nm molecular Doppler lidar. Optics Letters 25, 1231-1233.

Herbst, J., and Vrancken, P.: Design of a monolithic Michelson interferometer for fringe imaging in a near-field, UV, direct-detection Doppler wind lidar, Appl. Opt., 55(25), 6910-6929, https://doi.org/10.1364/AO.55.006910, 2016.

Hildebrand, J., Baumgarten, G., Fiedler, J., Hoppe, U. P., Kaifler, B., Lübken, F. J., and Williams, B. P.: Combined wind measurements by two different lidar instruments in the Arctic middle atmosphere, Atmos. Meas. Tech., 5, 2433-2445, https://doi.org/10.5194/amt-5-2433-2012, 2012.

Korb, C. L., Gentry, B. M., and Weng, C. Y.: Edge technique: theory and application to the lidar measurement of atmospheric wind, Appl. Opt., 31, 4202-4213, https://doi.org/10.1364/AO.31.004202, 1992.

Korb, C. L., Gentry, B. M., Li, S. X., and Flesia, C.: Theory of the double-edge technique for Doppler lidar wind measurement, Appl. Opt., 37, 3097-3104, https://doi.org/10.1364/AO.37.003097, 1998.

Lemmerz, C., Lux, O., Reitebuch, O., Witschas, B., and Wührer, C.: Frequency and timing stability of an airborne injection-seeded Nd: YAG laser system for direct-detection wind lidar, Appl. Opt., 56, 9057-9068, https://doi.org/10.1364/AO.56.009057, 2017.

Li, Z., Lemmerz, C., Paffrath, U., Reitebuch, O., and Witschas, B.: Airborne Doppler lidar investigation of sea surface reflectance at a 355-nm ultraviolet wavelength, J. Atmos. Oceanic Technol., 27, 693-704, https://doi.org/10.1175/2009JTECHA1302.1, 2010.

Liu, Z. S., Wu, D., Liu, J. T., Zhang, K. L., Chen, W. B., Song, X. Q., Hair, J. W., and She, C. Y.: Low-altitude atmospheric wind measurement from the combined Mie and Rayleigh backscattering by Doppler lidar with an iodine filter, Appl. Opt., 41, 7079-7086, https://doi.org/10.1364/AO.41.007079, 2002.

Lux, O., Lemmerz, C., Weiler, F., Marksteiner, U., Witschas, B., Rahm, S., Schäfler, A., and Reitebuch, O.: Airborne wind lidar observations over the North Atlantic in 2016 for the pre-launch validation of the satellite mission Aeolus, Atmos. Meas. Tech., 11, 3297-3322, https://doi.org/10.5194/amt-11-3297-2018, 2018.

Marksteiner, U.: Airborne wind lidar observations for the validation of the ADM-Aeolus instrument, Ph.D. thesis, Technische Universität München, 176 pp., 2013.

Marksteiner, U., Lemmerz, C., Lux, O., Rahm, S., Schäfler, A., Witschas, B., and Reitebuch, O.: Calibrations and Wind Observations of an Airborne Direct-Detection Wind LiDAR Supporting ESA's Aeolus Mission, Remote Sens., 10, 2056, https://doi.org/10.3390/rs10122056, 2018.

McGill, M. J., and Spinhirne, J. D.: Comparison of two direct-detection Doppler lidar techniques. Opt. Eng., 37(10), 2675-2686, https://doi.org/10.1117/1.601804, 1998.

McKay, J. A.: Modeling of direct detection Doppler wind lidar. II. The fringe imaging technique. Appl. Opt., 37, 6487-6493, https://doi.org/10.1364/AO.37.006487, 1998.

McKay, J. A., and Rees, D. J.: High-performance Fabry-Perot etalon mount for spaceflight. Opt. Eng., 39(1), 315-319, https://doi.org/10.1117/1.602361, 2000a.

McKay, J. A., and Rees, D.; Space-based Doppler wind lidar: modeling of edge detection and fringe imaging Doppler analyzers. Adv. Space. Res., 26(6), 883-891, https://doi.org/10.1016/S0273-1177(00)00026-0, 2000b.

McKay, J. A.: Assessment of a multibeam Fizeau wedge interferometer for Doppler wind lidar, Appl. Opt., 41, 1760-1767, https://doi.org/10.1364/AO.41.001760, 2002.

Pan, X., Shneider, M. N., and Miles, R. B.: Coherent Rayleigh-Brillouin scattering in molecular gases. Phys. Rev. A, 69, 033814, https://doi.org/10.1103/PhysRevA.69.033814 , 2004.

Paffrath, U., Lemmerz, C., Reitebuch, O., Witschas, B., Nikolaus, I., and Freudenthaler, V.: The airborne demonstrator for the direct-detection Doppler wind lidar ALADIN on ADM-Aeolus. Part II: Simulations and Rayleigh Receiver Radiometric performance, J. Atmos. Oceanic Technol., 26, 2516-2530, https://doi.org/10.1175/2009JTECHA1314.1, 2009.

Reitebuch, O., Lemmerz, C., Nagel, E., Paffrath, U., Durand, Y., Endemann, M., Fabre. F., and Chaloupy, M.: The airborne demonstrator for the direct-detection Doppler wind lidar ALADIN on ADM-Aeolus. Part I: Instrument design and comparison to satellite instrument, J. Atmos. Oceanic Technol., 26, 2501-2515, https://doi.org/10.1175/2009JTECHA1309.1, 2009.

Reitebuch, O.: Wind Lidar for Atmospheric Research, in: Atmospheric physics: Background, M~~m~~ethods, T~~t~~rends, edited by: Schumann, U., Research Topics in Aerospace, Springer, Berlin, London, 487–507, 2012a.

Reitebuch, O.: The space-borne wind lidar mission ADM-Aeolus. In Atmospheric Physics – Background, Methods, Trends, edited by Schumann, U., Research Topics in Aerospace. Springer, Berlin, London, 815-827, 2012b

Reitebuch, O., Huber, D., and Nikolaus, I.: ADM-Aeolus Algorithm Theoretical Basis Document (ATBD) Level1B Products, AE-RPDLR-L1B-001, 4.4, 117 pp., 2018.

Rennie, M., Tan, D., Andersson, E., Poli, P., Dabas, A., Kloe, J. D., Marseille, G. J., Stoffelen, A.: Aeolus Level-2B Algorithm Theoretical Basis Document, AE-TN-ECMWF-L2BP-0023, 3.0, 109 pp., 2017.

Schäfler, A., Craig, G., Wernli, H., Arbogast, P., Doyle, J. D., McTaggart-Cowan, R., Methven, J., Rivière, G., Ament, F., Boettcher, M., Bramberger, M., Cazenave, Q., Cotton, R., Crewell, S., Delanoë, J., Dörnbrack, A., Ewald, F., Fix, A., Gray, S. L., Grob, H., Groß, S., Hagen, M., Harvey, B., Hirsch, L., Jacob, M., Kölling, T., Konow, H., Lemmerz, C., Lux, O., Magnusson, L., Mayer, B., Mech, M., Moore, R., Pelon, J., Quinting, J., Rahm, S., Rapp, M., Rautenhaus, M., Reitebuch, O., Reynolds, C. A., Sodemann, H., Spengler, T., Vaughan, G., Wendisch, M., Wirth, M., Witschas, B., Wolf, K., and Zinner. T.: The N~~n~~orth A~~a~~tlantic W~~w~~aveguide and D~~d~~ownstream I~~i~~mpact E~~e~~xperiment, Bull. Am. Meteorol. Soc., 99, 1607-1637, 2018.

She, C. Y., Yue, J., Yan, Z. A., Hair, J. W., Guo, J. J., Wu, S. H., and Liu, Z. S.: Direct-detection Doppler wind measurements with a Cabannes–Mie lidar: A. Comparison between iodine vapor filter and Fabry–Perot interferometer methods, Appl. Opt., 46, 4434-4443, https://doi.org/10.1364/AO.46.004434, 2007.

Souprayen, C., Garnier, A., Hertzog, A., Hauchecorne, A., and Porteneuve, J.: Rayleigh–Mie Doppler wind lidar for atmospheric measurements. I. Instrumental setup, validation, and first climatological results, Appl. Opt., 38, 2410-2421, https://doi.org/10.1364/AO.38.002410, 1999a.

Souprayen, C., Garnier, A., and Hertzog, A.: Rayleigh–Mie Doppler wind lidar for atmospheric measurements. II. Mie scattering effect, theory, and calibration, Appl. Opt., 38, 2422-2431, https://doi.org/10.1364/AO.38.002422, 1999b.

Stoffelen, A., Pailleux, J., Källén, E., Vaughan, J. M., Isaksen, L., Flamant, P., Wergen, W., Andersson, E., Schyberg, H., Culoma, A., Meynart, R., and Ingmannt, P.: The atmospheric dynamics mission for global wind field measurement, Bull. Am. Meteorol. Soc., 86, 73-88, https://doi.org/10.1175/BAMS-86-1-73, 2005.

Sun, X. J., Zhang, R. W., Marseille, G. J., Stoffelen, A., Donovan, D., Liu, L., and Zhao, J.: The performance of Aeolus in heterogeneous atmospheric conditions using high-resolution radiosonde data, Atmos. Meas. Tech., 7, 2695-2717, https://doi.org/10.5194/amt-7-2695-2014, 2014.

Tan, D. G., Andersson, E., Kloe, J. D., Marseille, G. J., Stoffelen, A., Poli, P., Denneulin, M. L., Dabas, A., Huber, D., Reitebuch, O., Flamant, P., Le Rille, O., and Nett, H.: The ADM-Aeolus wind retrieval algorithms, Tellus A: Dyn. Meteorol. Oceanogr., 60, 191-205, https://doi.org/10.1111/j.1600-0870.2007.00285.x, 2008.

Tenti, G., Boley, C. D., and Desai, R. C.: On the kinetic model description of Rayleigh–Brillouin scattering from molecular gases, Can. J. Phys., 52, 285-290, https://doi.org/10.1139/p74-041, 1974.

Thuillier, G., and Hersé, M.: Thermally stable field compensated Michelson interferometer for measurement of temperature and wind of the planetary atmospheres, Appl. Opt., 30, 1210-1220, https://doi.org/10.1364/AO.30.001210, 1991.

Tucker, S. C., Weimer, C. S., Baidar, S., and Hardesty, R. M.: The Optical Autocovariance Wind Lidar. Part I: OAWL Instrument Development and Demonstration, J. Atmos. Oceanic Technol., 35, 2079-2097, https://doi.org/10.1175/JTECH-D-18-0024.1, 2018.

Wang, Z., Liu, Z., Liu, L., Wu, S., Liu, B., Li, Z., and Chu, X.: Iodine-filter-based mobile Doppler lidar to make continuous and full-azimuth-scanned wind measurements: data acquisition and analysis system, data retrieval methods, and error analysis, Appl. Opt., 49, 6960-6978, https://doi.org/10.1364/AO.49.006960, 2010.

Weiler, F.: Bias correction using ground echoes for the airborne demonstrator of the wind lidar on the ADM-Aeolus mission, Master's thesis, University of Innsbruck, 96 pp., available at: https://resolver.obvsg.at/urn:nbn:at:at-ubi:1-7104 (last access: 11 October 2017), 2017.

Weissmann, M., and Cardinali, C.: Impact of airborne Doppler lidar observations on ECMWF forecasts, Q. J. R. Meteorolog. Soc., 133, 107-116, https://doi.org/10.1002/qj.16, 2007.

Witschas, B.: Analytical model for Rayleigh–Brillouin line shapes in air, Appl. Opt., 50, 267-270,https://doi.org/10.1364/AO.50.000267, 2011a.

Witschas, B.: Analytical model for Rayleigh–Brillouin line shapes in air: errata, Appl. Opt., 50, 5758-5758, https://doi.org/10.1364/AO.50.005758, 2011b.

Witschas, B.: Experiments on spontaneous Rayleigh-Brillouin scattering in air, PhD thesis, Friedrich-Schiller-Universität, Jena, 112 pp., available at: http://elib.dlr.de/98547/ (last access: 8 March 2017), 2011 (c).

Witschas, B., Lemmerz, C., and Reitebuch, O.: Horizontal lidar measurements for the proof of spontaneous Rayleigh–Brillouin scattering in the atmosphere, Appl. Opt., 51, 6207-6219, https://doi.org/10.1364/AO.51.006207, 2012.

Witschas, B., Lemmerz, C., and Reitebuch, O.: Daytime measurements of atmospheric temperature profiles (2–15 km) by lidar utilizing Rayleigh–Brillouin scattering, Opt. Lett., 39, 1972-1975,https://doi.org/10.1364/OL.39.001972, 2014.

Xia, H., Dou, X., Sun, D., Shu, Z., Xue, X., Han, Y., Hu, D., Han, Y., and Cheng, T.: Mid-altitude wind measurements with mobile Rayleigh Doppler lidar incorporating system-level optical frequency control method, Opt. Express, 20, 15286-15300, https://doi.org/10.1364/OE.20.015286, 2012.

Žagar, N., Stoffelen, A., Marseille, G. J., Accadia, C., and Schlüssel, P.: Impact assessment of simulated Doppler wind lidars with a multivariate variational assimilation in the tropics, Mon. Weather Rev., 136, 2443-2460, https://doi.org/10.1175/2007MWR2335.1, 2008.

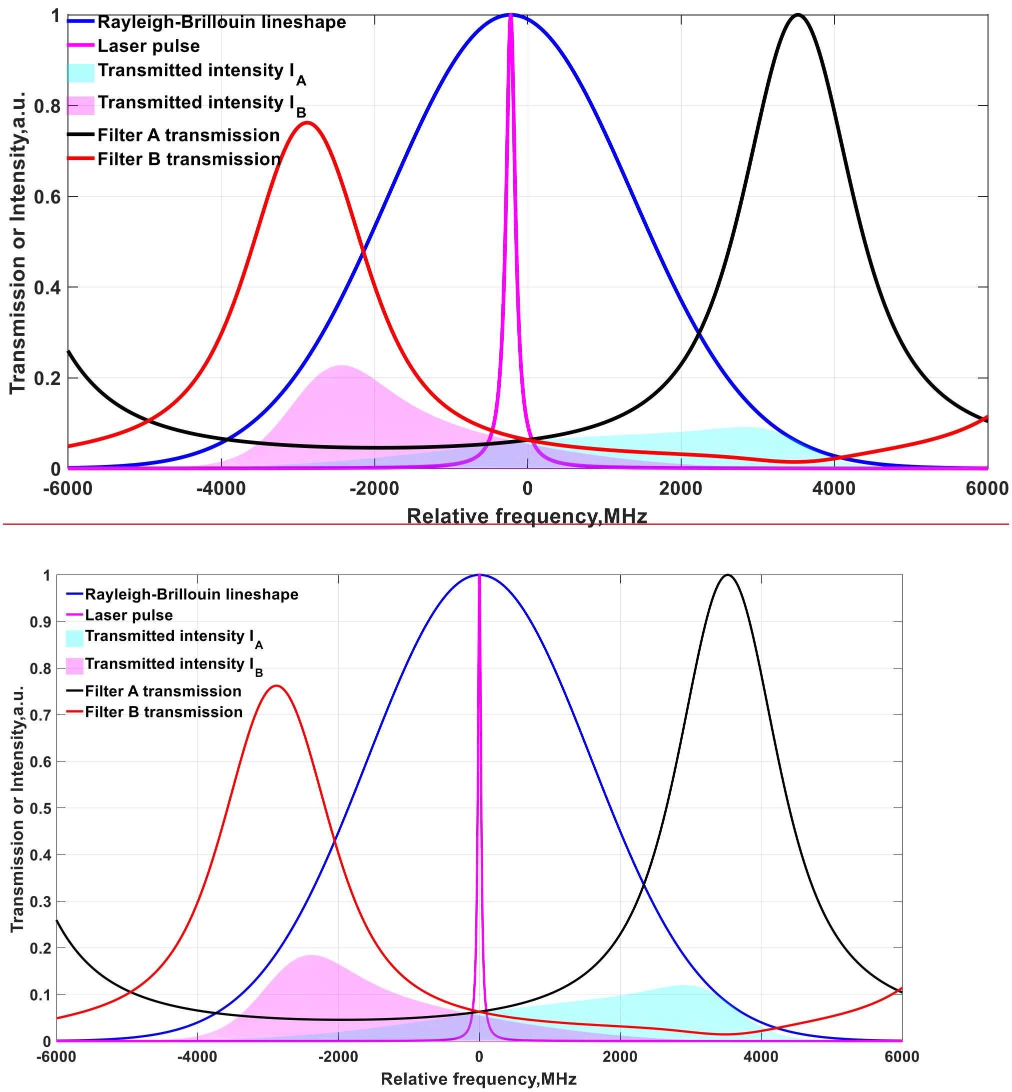

Figure 1: Modelled spectral distribution of the transmitted laser pulse (pink line) and pure molecular backscatter (blue line) for T=270 K, P=700 hPa normalized to one. The Rayleigh channel transmission spectra of two FPIs are shown in black T_A (*f*) and red T_B (*f*) lines, respectively. The transmitted integrated intensities through FPI A and B are marked with light blue and magenta filled areas.

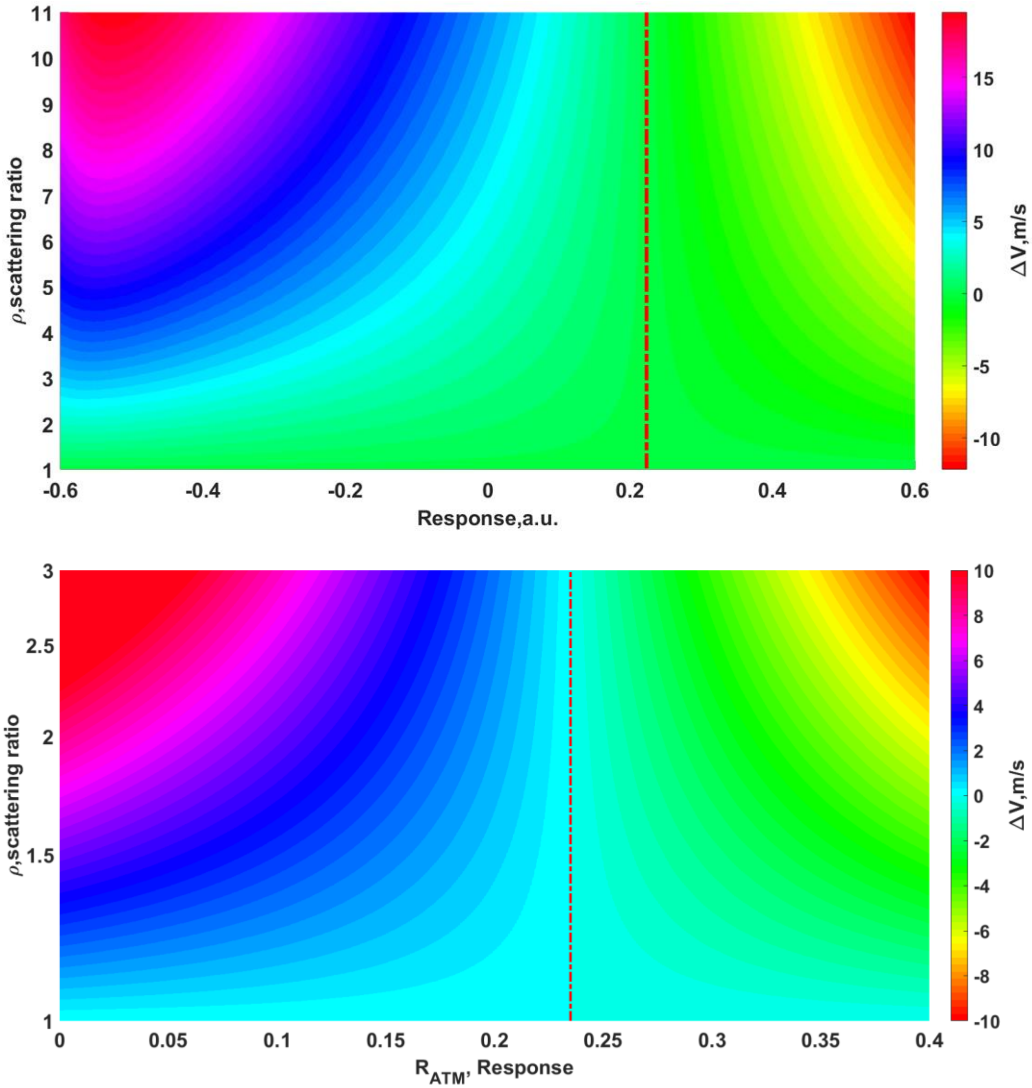

Figure 2: Simulation of LOS wind velocity errors ΔV_{MC} induced~~generated~~ by Mie contamination and a molecular lineshape at T=223 K and P=301 hPa. The *x*-axis and *y*-axis represent the response value R_{ATM} and scattering ratio ρ , respectively. The red dashed-line corresponds to the response value with minimum ΔV_{MC}~~ΔV~~ at each scattering ratio.

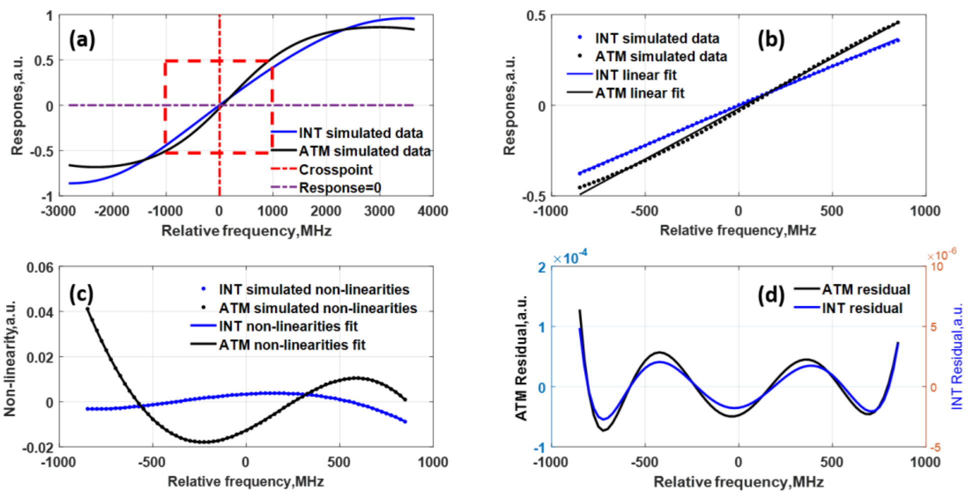

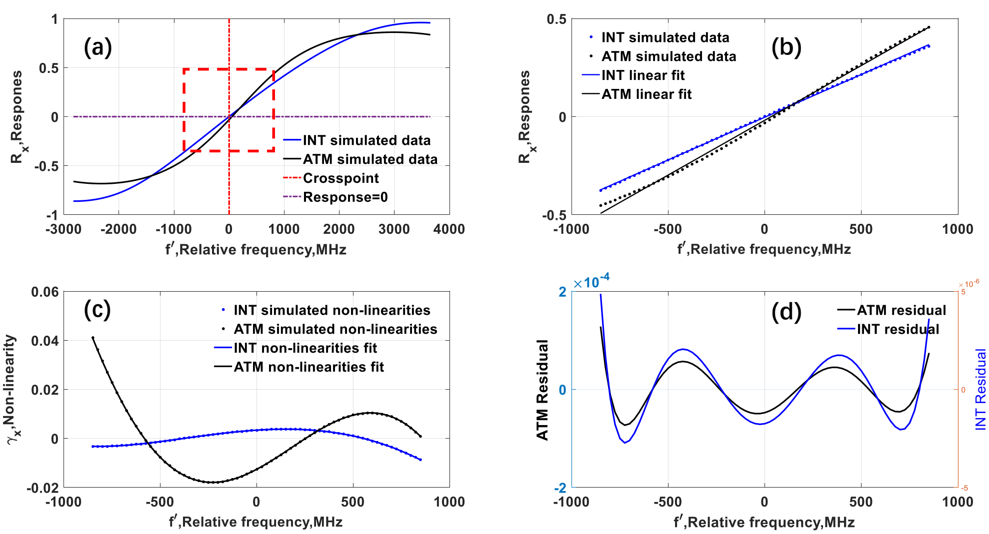

Figure 3: (a) ~~The~~ Simulated Rayleigh Response Calibration (SRRC) for internal reference (INT, blue line) and atmospheric return (ATM, black line), the cross point frequency is marked by~~with~~ red dotted~~-~~ line, (b) INT (blue dots) and ATM (black dots) response functions and corresponding linear least squares fits (blue line for INT, black line for ATM) ~~calibration with~~over a frequency interval of ±850 MHz, where relative frequency is used instead of absolute ~~frequencies~~frequency, (c) ~~the~~ simulated non-linearities ~~of simulated~~ (dots) and ~~fitted (lines) response functions from~~ 5^{th} order polynomial fits for INT (blue line) and ATM (black line). (d) response function residuals from INT (blue line) and ATM (black line).

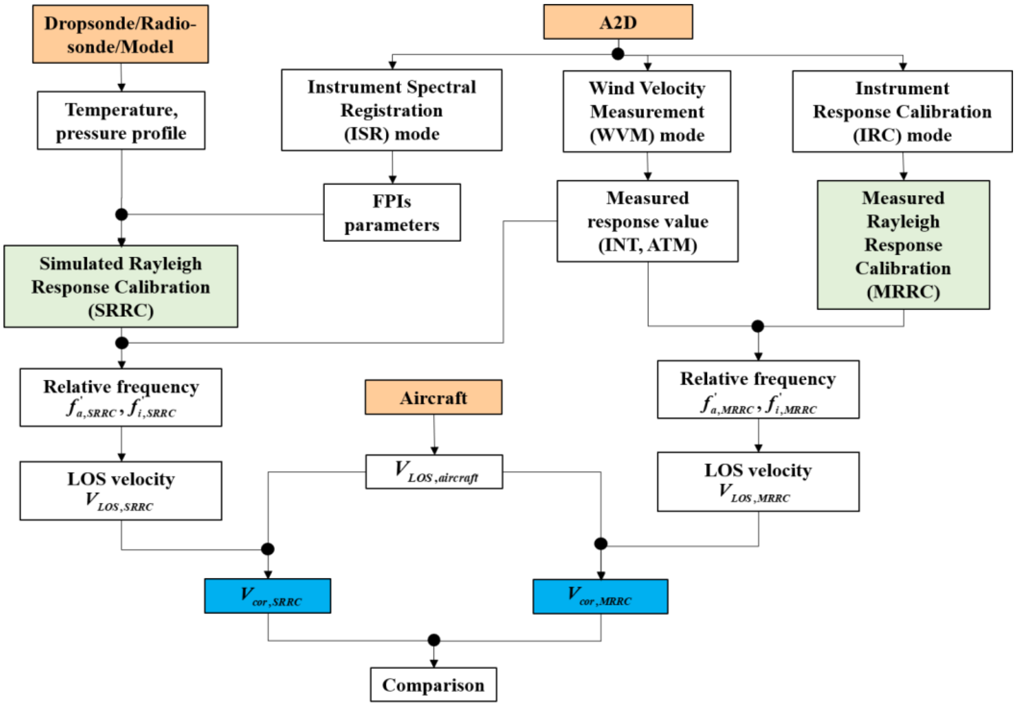

Figure 4: Flowchart of LOS velocity retrieval and comparison between A2D SRRC and MRRC.

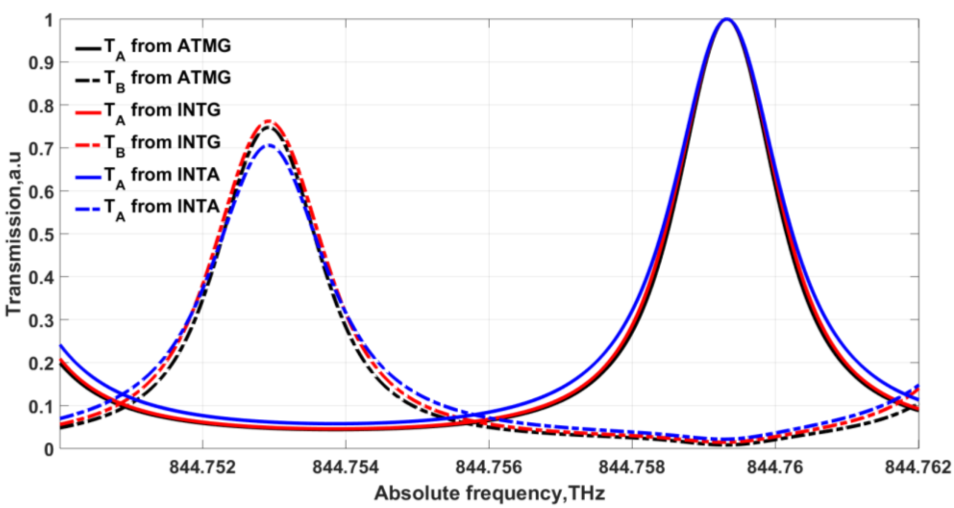

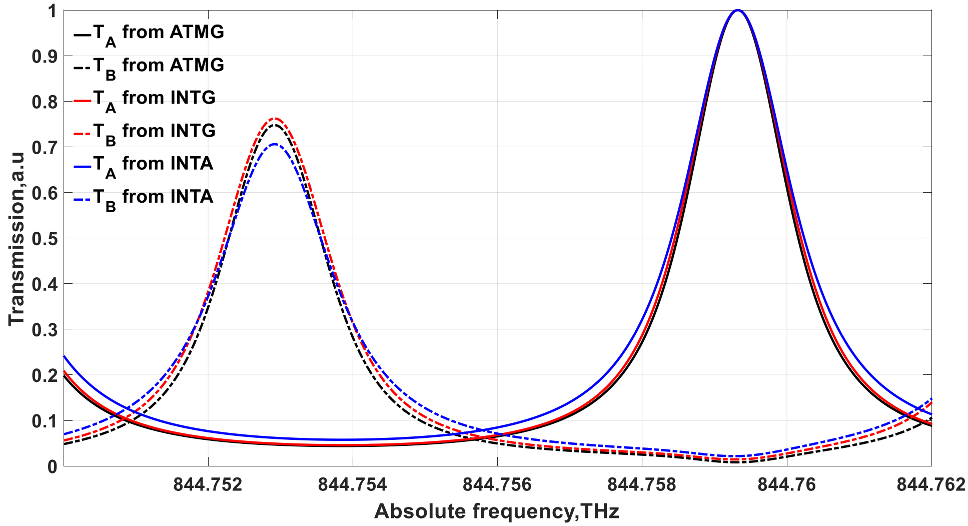

Figure 5: The transmission function of fitted ~~fitsting of~~ FPIs from different campaigns and detection channels. The black, red and blue groups are obtained from ATM path measurement during BRAINS ground campaign (ATMG) in 2009, INT path measurement during NAWDEX from ground (INTG) in 2016 and INT path measurement during NAWDEX airborne measurement (INTA) in 2016, respectively.

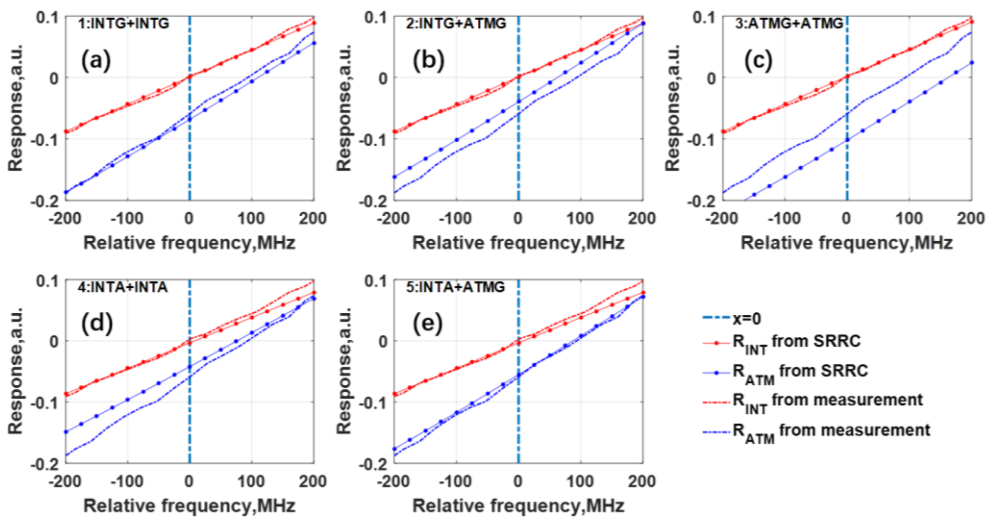

Figure 6: The response functions of internal reference and 8th atmospheric ~~range gate~~altitude bin from MRRC (red and blue dashed-lines, respectively, same on every plot) and different SRRCs using different combinations of FPIs transmission parameters (red and blue dotted-lines, respectively) a listed in T~~t~~able 4.

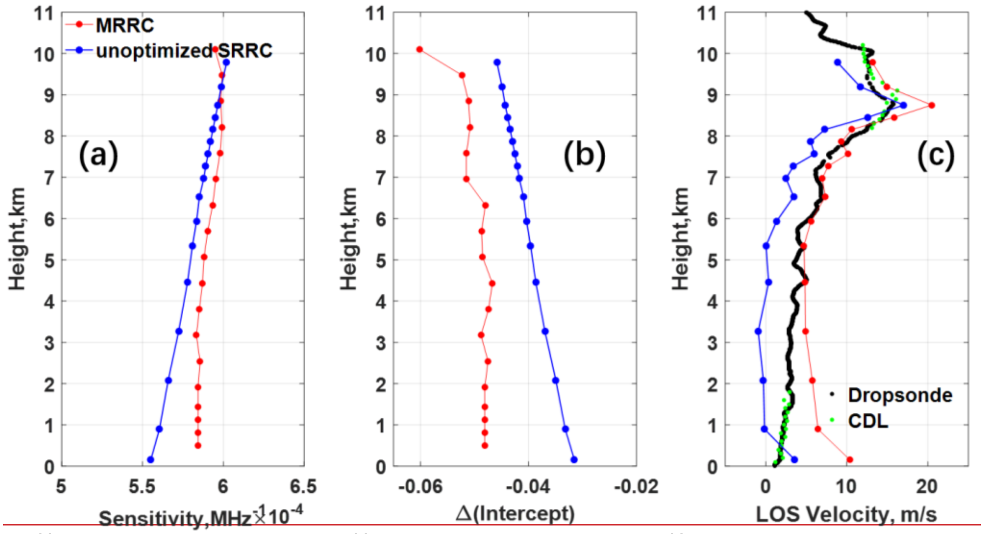

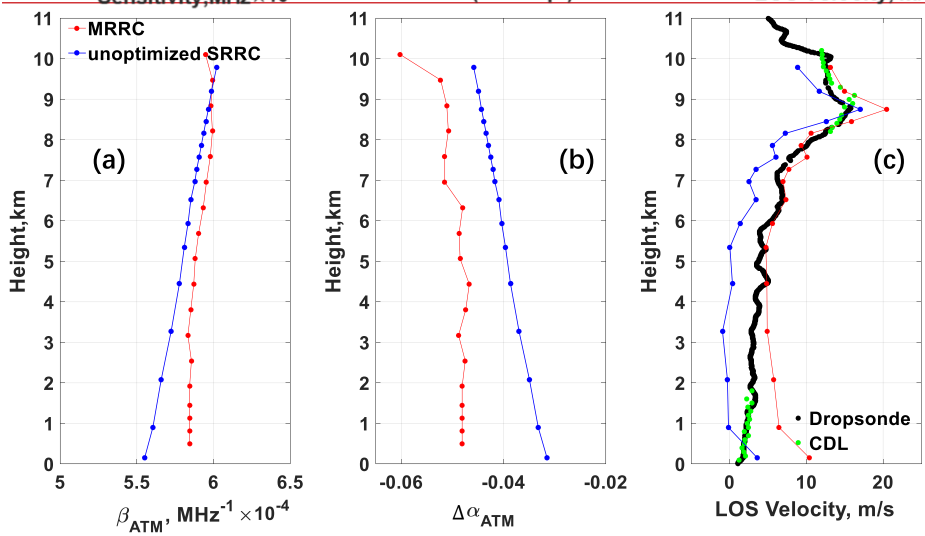

Figure 7: Case study using dropsonde data on 08:27:07 UTC, 23 September 2016: Comparison of (a) sensitivity β_{ATM} (MHz^{-1}) (b) $\Delta\alpha_{ATM}$ ~~intercept~~ α_{ATM} (c) LOS velocity between results from A2D Rayleigh channel MRRC (red) and not ~~un~~optimized SRRC (blue). The LOS velocity from dropsonde (black) and CDL (green) are also presented in Fig. 7 (c).

~~**Figure 7: Case study using dropsonde data on 08:27:07 UTC, 23 September 2016: Comparison of (a) sensitivity (b) intercept (c) LOS velocity between results from A2D Rayleigh channel MRRC (red) and unoptimized SRRC (blue). The LOS velocity from dropsonde (black) and CDL (green) are also presented in Fig. 7 (c).**~~

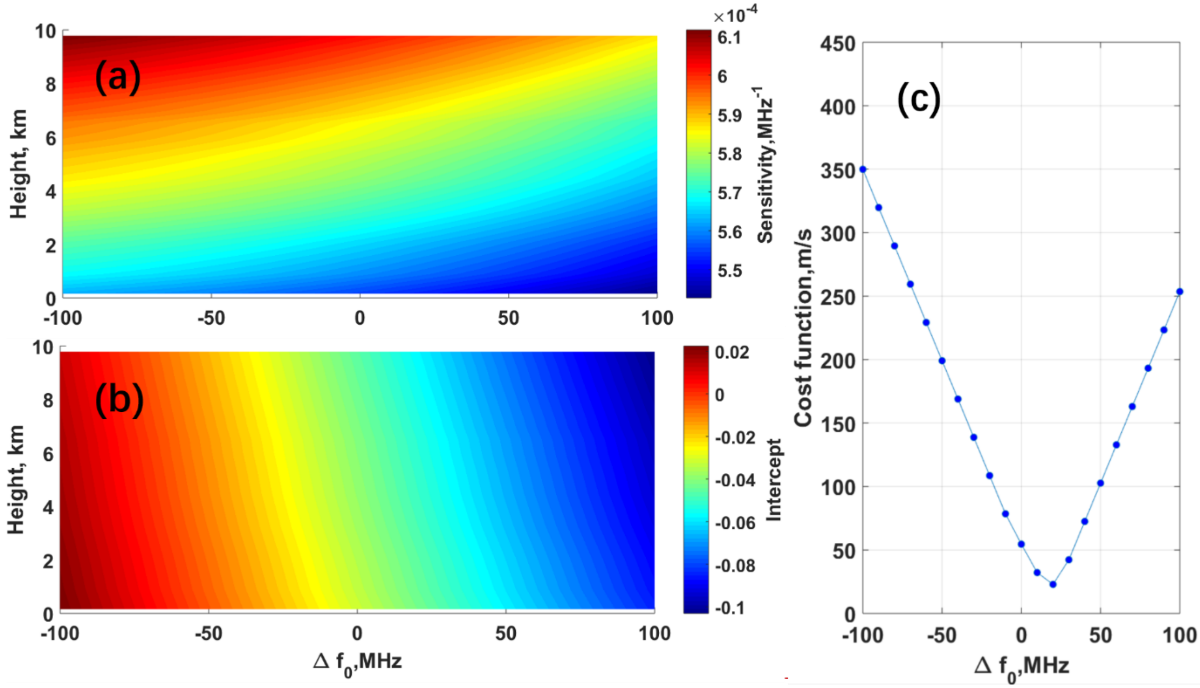

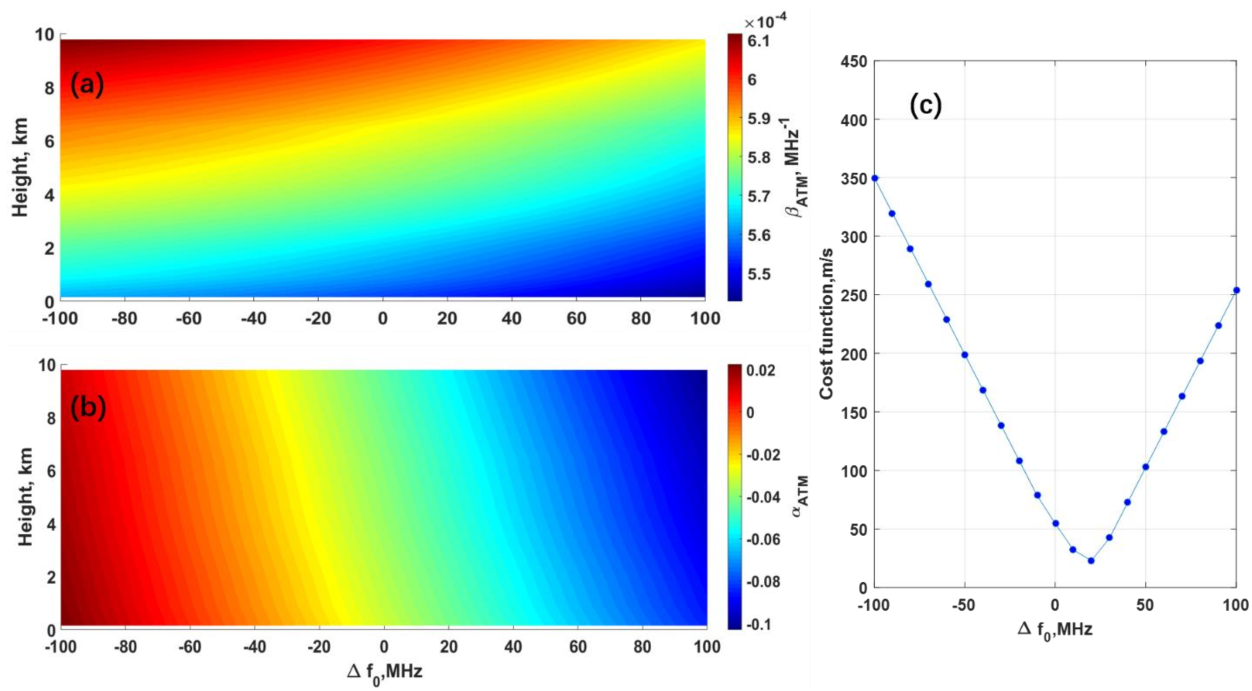

Figure 8: The effect of the centre frequency offset Δf_0 of filter A and B for atmospheric path on atmospheric response (a) β_{ATM} (b) α_{ATM} and (c) corresponding cost function $F(\Delta f_0)$.

~~Figure 8: The effect of the centre frequency offset Δf_0 of filter A and B for atmospheric path on atmospheric response (a) β_{ATM} (b) α_{ATM} and (c) corresponding cost function $F(\Delta f_0)$.~~

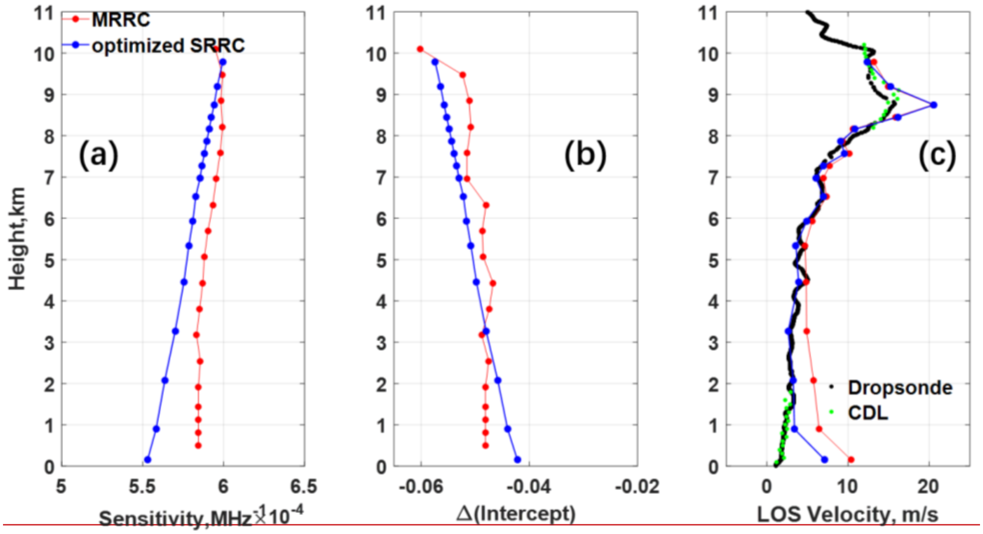

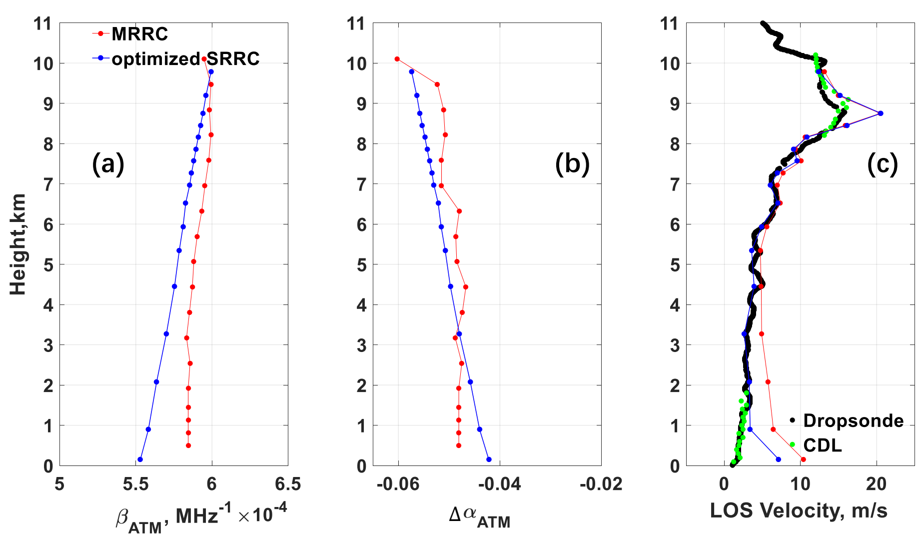

Figure 9: Case study using dropsonde data on 08:27:07 UTC, 23 September 2016: Comparison of (a) sensitivity β_{ATM} (MHz^{-1}) (b) ~~intercept~~ $\Delta\alpha_{ATM}$ (c) retrieved LOS velocity between results from A2D Rayleigh channel MRRC (red) and optimized SRRC (blue). The LOS velocity from dropsonde (black) and CDL (green) are also presented in Fig. 9 (c).

~~Figure 9: Case study using dropsonde data on 08:27:07 UTC, 23 September 2016: Comparison of (a) sensitivity (b) intercept (c) LOS velocity between results from A2D Rayleigh channel MRRC (red) and optimized SRRC (blue). The LOS velocity from dropsonde (black) and CDL (green) are also presented in Fig. 9 (c).~~

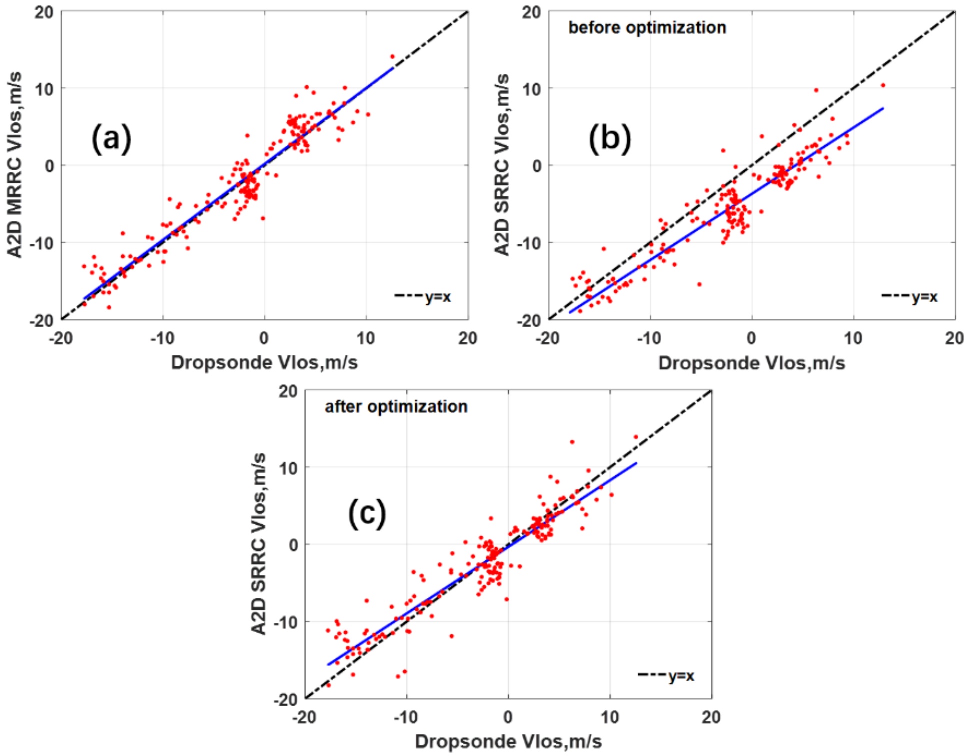

Figure 10: LOS velocity comparison obtained from (a) dropsonde and A2D Rayleigh channel measurement with MRRC (b) dropsonde and SRRC before FPIs optimization and (c) dropsonde and SRRC after FPIs optimization.

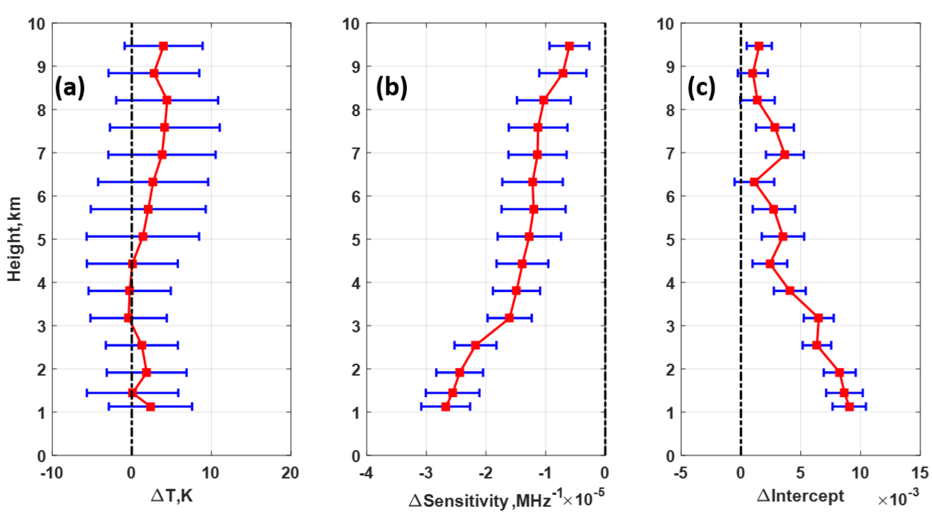

Figure 11: (a) Difference of temperature between dropsondes used in SRRC and the one during A2D instrument response calibration, and the difference of (b) sensitivity (c) intercept derived from A2D SRRC and MRRC. The red square and the blue bar represent the mean bias and standard deviation at each height.

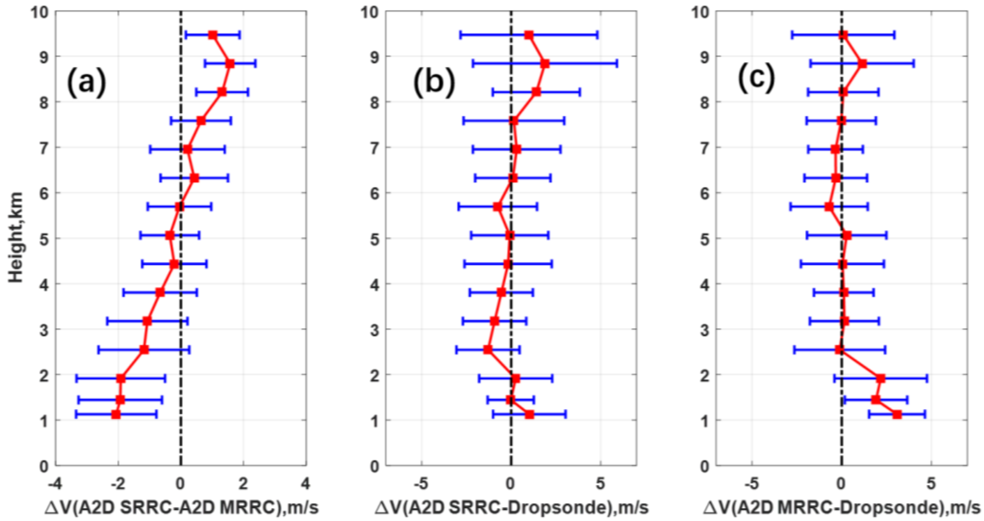

Figure 12: ~~The c~~Comparison of profiles for~~of~~ LOS velocity (a) between A2D SRRC and MRRC (b) SRRC and dropsonde (c) MRRC and dropsonde.

~~Figure 12: Difference inThe comparison profiles of LOS velocityprofiles (a) between A2D SRRC and MRRC (b) SRRC and dropsonde (c) MRRC and dropsonde.~~

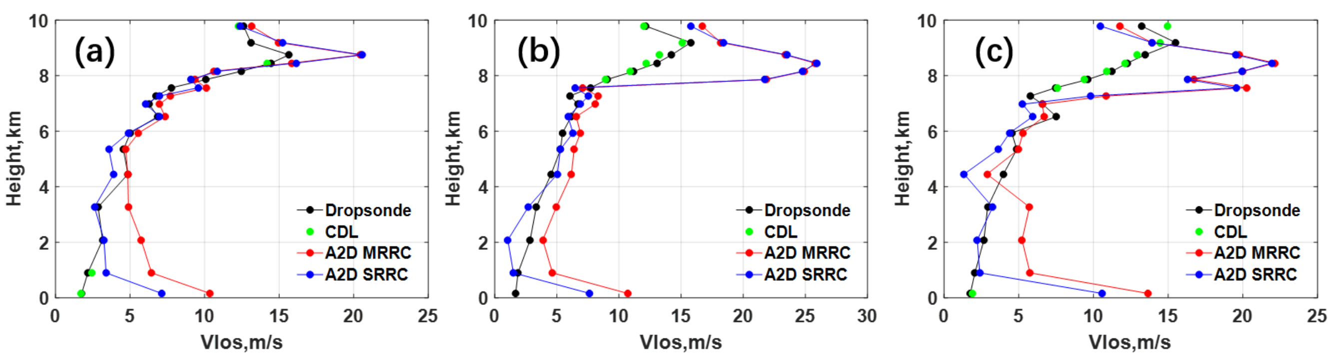

Figure 13: LOS velocity from dropsonde (black), CDL (green), A2D MRRC (red) and A2D SRRC (blue) on (a) 08:27:07 UTC (b) 08:33:06 UTC (c) 08:39:05 UTC, 23 September 2016.

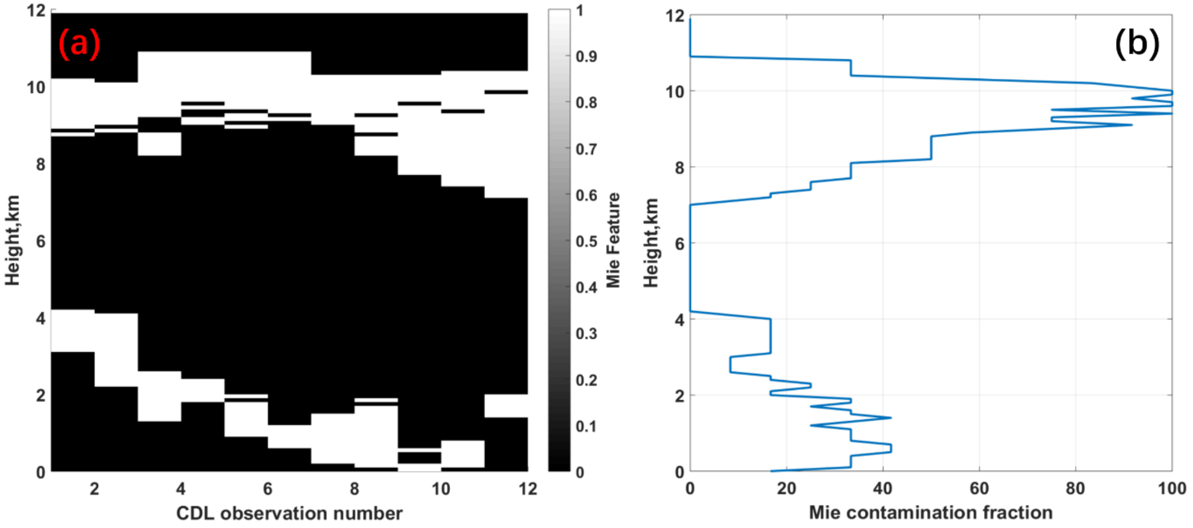

Figure 14: (a) Matched CDL measurement ~~behaviour~~ where valid (or invalid) signal is represented as 1 (or 0) (b) Mie contamination fraction F_{Mie} of selected datasets from Table 2 used for comparison ~~analysis~~.

Table 1. Comparison of different FPI-based direct detection wind lidars

Lidar	Wavelength and system	Calibration approach	Instrument drift via correction	References
OHP [a] Rayleigh lidar	532 nm, double FPIs	Simulation, FPI scan~~ning~~	quick wind acquisition cycle strategy	Chanin et al., 1989; Garnier and Chanin, 1992; Souprayen et al., 1999a, 1999b
NASA [b] Rayleigh/Mie lidar	355 nm, three FPIs	Simulation, FPI or laser frequency scan~~ning~~	locking etalon and servo-control system	Korb et al., 1992; Korb et al. 1998; Flesia and Korb, 1999; ~~Flesia et al., 2000~~ Gentry et al. 2000
USTC [c] Rayleigh lidar	355 nm, three FPIs	measurement and simulation, FPI scan~~ning~~	locking etalon and servo-control system	Xia et al., 2012; Dou et al., 2014
ESA ALADIN	355 nm, double FPIs for Rayleigh channel	level 1B: measurement, laser scanning level 2B: simulation, laser frequency scan~~ning~~	internal reference path	Reitebuch et al., 2018; Rennie et al., 2017
DLR A2D	355 nm, double FPIs for Rayleigh channel	Measurement, laser frequency scan~~ning~~	internal reference path	Marksteiner, 2013; Lux et al., 2018; Marksteiner et al., 2018

[a] Observatory of Haute Provence, France

[b] National Aeronautics and Space Administration, U.S.

[c] University of Science and Technology of China, China. This lidar is mobile.

Table 2: Overview of analysed datasets from A2D, 2 µm CDL and dropsonde in the frame of the NAWDEX campaign.

Date	A2D measurement period (UTC) and mode	Data availability of CDL	Matched dropsonde Time (UTC)
17.09.2016	10:30-11:35 Wind measurement	available	11:09:15 11:33:47
	11:42-12:24 Wind measurement	no data	11:56:00 12:05:20 12:15:02 12:24:23
21.09.2016	15:34-15:57 Wind measurement	available	15:40:49 15:45:07 15:48:34 15:52:51
23.09.2016	07:51-08:53 Wind measurement	available	08:19:01 08:27:07 08:33:06 08:39:05 08:45:05 08:51:16
28.09.2016	12:53 - 13:17 Calibration	available	No data
18.10.2016	09:20-09:57 Wind measurement	not available	09:22:48 09:27:15 09:31:53 09:36:29 09:52:30

Table 3: Specific parameters of FPIs during different ground and airborne campaigns illustrated in Fig. 5

Parameters	ATM Ground ATMG		INT Ground INTG		INT Airborne INTA	
Filters	filter A	filter B	filter A	filter B	filter A	filter B
FSR (GHz)	10.934	10.998	10.934	10.851	10.934	10.934
FWHM (GHz)	1.671	1.733	1.743	1.847	1.833	1.943
R	0.670	0.696	0.668	0.679	0.622	0.610
σ_g (MHz)	266	363	303	391	210	247

Table 4: Combinations for internal reference and atmospheric response simulation with ε_{R_slope} and $\varepsilon_{R\_intercept}$ ~~slope and intercept values of ε_R linear fit calculated~~ based on Eqs. (18A) – (18B) (Dabas and Huber, 2017).

Combination	Internal reference response	Atmospheric response	ε_{R_slope} ~~Slope~~ ~~Aslope?~~	$\varepsilon_{R\_intercept}$ ~~Intercept~~ ~~Aintercept~~
1	INTG	INTG	-1.48×10^{-5}	-0.0057
2	INTG	ATMG	-1.42×10^{-7}	0.0206
3	ATMG	AMTG	-1.39×10^{-5}	-0.0356
4	INTA	INTA	-7.74×10^{-5}	0.0181
5	INTA	ATMG	-9.02×10^{-7}	0.0059

Table 5: Statistical comparison between results from dropsonde, A2D Rayleigh channel measurement and SRRC before and after FPIs optimization during 2016 campaign.

Statistical parameters	Dropsonde to A2D MRRC	Dropsonde to A2D SRRC before FPIs optimization	Dropsonde to A2D SRRC after FPIs optimization
Number of compared data pairs	185	190	190
Correlation coefficient-, *r*	0.95	0.93	0.94
Slope	0.99	0.86	0.86
Intercept, m s^{-1}	0.19	-3.70	-0.32
Mean bias, m s^{-1}	0.23	-3.32	0.05
Standard deviation, m s^{-1}	2.20	2.61	2.52